PREPARED FOR
AIR FORCE OFFICE OF SCIENTIFIC RESEARCH/NA
BLDG 410
BOLLING AIR FORCE BASE, DC 20332

FZM-6661
March 1977

12

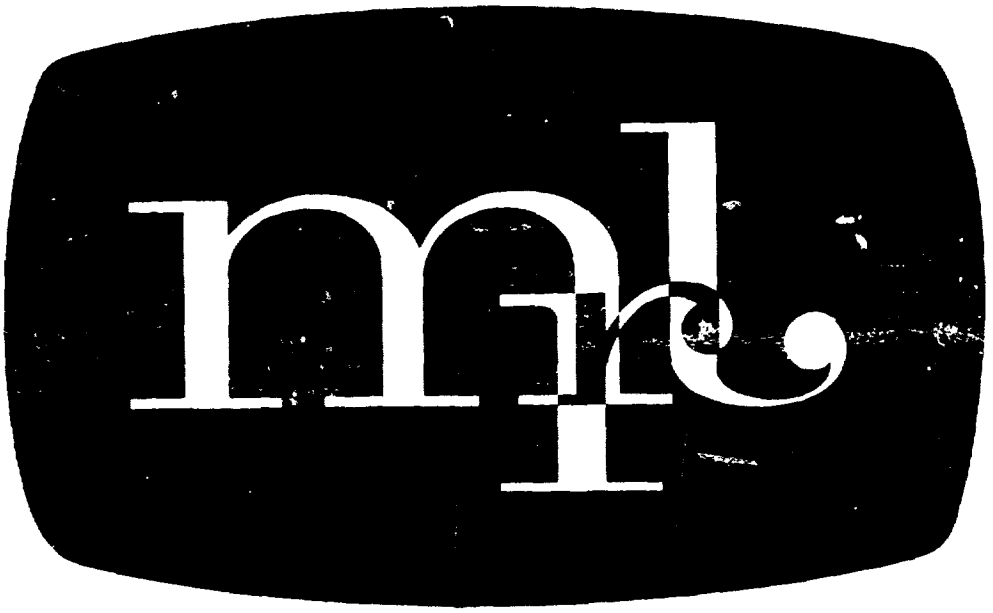

MATERIALS RESEARCH LABORATORY

RESPONSE OF GRAPHITE COMPOSITES TO LASER RADIATION

FINAL SCIENTIFIC REPORT
1 February 1976 to 30 April 1977
Contract F44620-76-C-0030

K.G. Kibler, H.G. Carter, J.R. Eisenmann

GENERAL DYNAMICS
Fort Worth Division

P.O. Box 748 Fort Worth, Texas 76101

AIR FORCE OFFICE OF SCIENTIFIC RESEARCH (AFSC)
NOTICE OF TRANSMITTAL TO DDC
This technical report has been reviewed and is approved for public release IAW AFR 190-12 (7b).
Distribution is unlimited.
A. D. BLOSE
Technical Information Officer

UNCLASSIFIED

SECURITY CLASSIFICATION OF THIS PAGE (When Data Entered)

REPORT DOCUMENTATION PAGE	READ INSTRUCTIONS BEFORE COMPLETING FORM
1. REPORT NUMBER: AFOSR-TR- [illegible] 2. GOVT ACCESSION NO.	3. RECIPIENT'S CATALOG NUMBER
4. TITLE (and Subtitle): RESPONSE OF GRAPHITE COMPOSITES TO LASER RADIATION, FINAL SCIENTIFIC REPORT, 1 February 1976 to 30 April 1977	5. TYPE OF REPORT & PERIOD COVERED: FINAL, 1 Feb 1976 - 30 April 1977 6. PERFORMING ORG. REPORT NUMBER: FZM-6661
7. AUTHOR(s): K.G. KIBLER, H.G. CARTER, J R EISENMANN	8. CONTRACT OR GRANT NUMBER(s): F44620-76-C-0030
9. PERFORMING ORGANIZATION NAME AND ADDRESS: GENERAL DYNAMICS CORPORATION, FORT WORTH DIVISION/PO BOX 748, FORT WORTH, TX 76101	10. PROGRAM ELEMENT, PROJECT, TASK AREA & WORK UNIT NUMBERS: 2307/B2, 61102F
11. CONTROLLING OFFICE NAME AND ADDRESS: AIR FORCE OFFICE OF SCIENTIFIC RESEARCH/NA, BLDG 410, BOLLING AIR FORCE BASE, D C 20332	12. REPORT DATE: March 1977 13. NUMBER OF PAGES: 104
14. MONITORING AGENCY NAME & ADDRESS (if different from Controlling Office)	15. SECURITY CLASS. (of this report): UNCLASSIFIED 15a. DECLASSIFICATION/DOWNGRADING SCHEDULE

16. DISTRIBUTION STATEMENT (of this Report)

Approved for public release; distribution unlimited.

17. DISTRIBUTION STATEMENT (of the abstract entered in Block 20, if different from Report)

18. SUPPLEMENTARY NOTES

19. KEY WORDS (Continue on reverse side if necessary and identify by block number)

GRAPHITE FIBER COMPOSITES
CO_2 LASER RADIATION
BURNTHROUGH DAMAGE
HEATING DAMAGE
RESIDUAL STRENGTH

20. ABSTRACT (Continue on reverse side if necessary and identify by block number)

Experimental and analytical investigations of the response of graphite-epoxy composite tensile coupons to laser radiation have been performed. Three different 5208/T300 laminates were used to compare stacking sequence effects, three thicknesses of one of the laminates were studied, and an aluminum alloy was employed for comparison purposes. The experimental program has concentrated on laser-induced controlled-depth damage, physical characterization of the damaged area, and residual tensile strength measurements. Thermal response measurements were conducted on selected specimens to aid in assessing the damage mechanisms

DD FORM 1 JAN 73 1473 EDITION OF 1 NOV 65 IS OBSOLETE

UNCLASSIFIED

SECURITY CLASSIFICATION OF THIS PAGE (When Data Entered)

and to formulate a penetration model. An additional feature of the experiments included laser exposure of preloaded specimens to determine the requisite "energy-to-fracture." By considering the material response in three different incident intensity ranges, we have delineated the interactions which occur and formulated models which predict the thermal response, mass ablation, and penetration in those ranges. The strength retention for partially-penetrated, laser-damaged composites is describable in terms of fracture-mechanics-based predictions at all but the lowest intensity investigated, where essentially only resin sublimation occurs. Painted aluminum is more susceptible than composites to damage at high intensity, while strength retentions are similar at intermediate intensities.

* There was

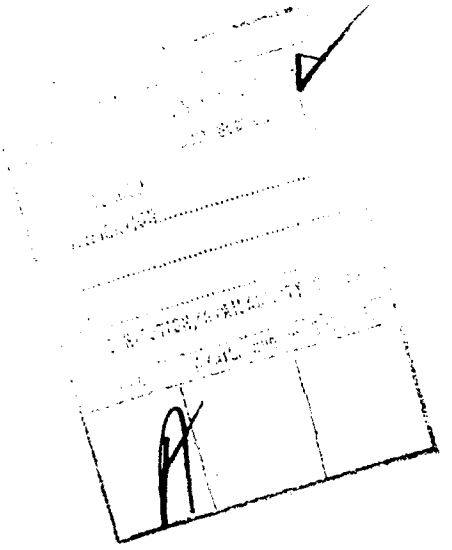

FOREWORD

The work reported herein was performed under the sponsorship of the Air Force Office of Scientific Research, Bolling Air Force Base, D. C. 20332, under AFOSR Contract F44620-76-C-0030. Mr. William J. Walker, AFOSR/NA, was the Air Force Program Manager.

The results described in this report summarize the technical effort accomplished in the contractual period from 1 February 1976 through 30 April 1977.

The work was performed by General Dynamics Corporation, Fort Worth Division, Fort Worth, TX 76101, with experimental assistance of the Laser Hardened Materials Evaluation Laboratory (LHMEL), AFML/LPJ, Wright-Patterson AFB, Ohio 45433. General Dynamics personnel who contributed to this program were K. G. Kibler (Principal Investigator), H. G. Carter (Thermal Analysis), J. R. Eisenmann and B. T. Rodini (Fracture Analysis) and R. H. McDaniel (Tensile Testing and Damage Analysis). Grateful acknowledgment is extended to D. F. Stevison, AFML/LPJ experiment coordinator, and the LHMEL support contractor staff, directed by J. M. Short.

TABLE OF CONTENTS

TABLE OF CONTENTS (Continued)

LIST OF FIGURES

LIST OF FIGURES (Continued)

LIST OF TABLES

LIST OF TABLES (Continued)

SUMMARY

We have conducted a series of experimental and analytical investigations on the response of graphite-epoxy composites to continuous-wave CO_2 laser radiation. This work was sponsored by the Air Force Office of Scientific Research under Contract F44620-76-C-0030. This final report details the investigations completed during the period 1 February 1976 to 30 April 1977.

The objectives of the program were to gain a basic understanding of the physical response of graphite-epoxy composites to laser radiation, compare the response to that of aluminum, and formulate simple models to predict the penetration susceptibility and strength degradation of laser-irradiated graphite-epoxy composites.

Tensile coupons of one graphite-epoxy system (Narmco 5208/T300) and one aluminum alloy (2024(T81)) have been exposed to laser radiation using the low power facility of General Dynamics and the Laser Hardened Materials Evaluation Laboratory (AFML) high power facilities. Three composite laminates, namely $(0/\pm45)_c$, $(\pm45/90)_{2S}$, and $(90/\pm45)_{2S}$, and three thicknesses of $(0/\pm45)_c$, namely $(0/\pm45)_S$, $(0/\pm45)_{2S}$, and $(0/\pm45)_{4S}$ were used. The experimental program has featured static irradiation of coupons with subsequent damage and residual strength characterization, irradiation-to-fracture of preloaded coupons, and thermal response characterization of laser heated specimens.

Correlations of our experimental data on temperature response, mass loss, and penetration time requires consideration of the incident laser intensity in three ranges, which we designate as low, intermediate, and high intensity. In the low intensity range our model applies only to composites. Mass loss there for exposure times on the order of seconds is primarily due to resin ablation. Mass loss and surface damage area are satisfactorily predicted as a function of exposure time and specimen thickness.

The transition from low to intermediate range response involves a "runaway" effect as the thermal conductivity along the length of the graphite fibers decreases with increasing temperature. Composite exposures in this range are characterized by an initial period of resin sublimation followed by fiber sublimation. Radiative emission is significant in this range. Order-of-magnitude agreement for mass ablation and penetration times are obtained by using our high intensity model.

The high intensity model for mass ablation applies both to composites and aluminum. The laser interaction here resembles a drilling process. Since power going into radiative emission is small compared to absorption by sublimation, mass ablation and penetration are characterized here by an effective heat of ablation.

Correlations of our composite residual strength data with laser exposure conditions demonstrates that, except at low intensity, the strength retention of laser-damaged composites is described by a parameter which involves incident energy density, incident beam radius, and specimen thickness. The results may be expressed in a dimensionless form which characterizes an effective transverse damage cross section, and thus may be related to conventional drilled holes, even though the laser-damaged specimens may suffer only partial penetration.

A fracture-mechanics based strength prediction based on notched control data adequately describes the strength retention of the $(0/\pm45)_c$ laminates at all intensities investigated, except the lowest. At low intensity, the damage is due primarily to resin sublimation and thus represents a different response both from a thermal and mechanical standpoint. Sublimation of resin from the outer plies does however significantly limit the tensile capability of the specimens.

The $(90/\pm45)_c$ results are generally predictable using the same parameterization as above, although the experimental data scatter is large. Different strength retentions were noted for the two different stacking sequences of this class of laminates, which indicates a sensitivity of the residual strength to near-surface ply orientation.

For high intensity beams, 2024(T81) aluminum is more easily penetrated than graphite-epoxy coupons of approximately equivalent undamaged strength. At low intensity, aluminum is not damaged. At intermediate intensities, the strength retentions for laser-damaged composites and aluminum are similar, while at high intensity the aluminum retention is significantly less than that for composites similarly exposed.

Preloaded composites and aluminum tend to fracture under high intensity exposure at loads equivalent to approximately 80-90% of the strength retention they would have if similarly exposed without load. If these specimens are not fractured, their residual strengths are similar to unloaded specimens which are equivalently irradiated.

1. INTRODUCTION

Although the use of composite materials has increased dramatically over the last decade, it is only in the very recent past that we have begun to appreciate the effects of "environment" on composites. Just as defect types and size have different implications for metals and non-metallic composite materials, so different environments have varied effects. In this report we deal with the response of graphite-epoxy materials to an extreme environment - intense local heating induced by laser.

The development of linear fracture mechanics and an extensive experimental data base permits the evaluation of fracture behavior of conventional metals. Although fracture mechanics-based concepts are being applied to composites, much work remains to be accomplished before damage-tolerant design concepts can fully mature.

Previous work initiated by General Dynamics several years ago (Ref. 1, 2) investigated the residual strength characteristics of a quasi-isotropic laminate exposed to laser beams of modest intensity. The interesting feature of that work was that although total penetration of the specimens did not occur, the strength retention was correlated with an appropriately defined "hole" size.

The work of Ender, et al (Ref. 3) is a notable example of investigations to compare the strength reduction of various materials, including graphite-epoxy composite, exposed to a range of laser beam intensities, beam spot sizes, and load effects. That work emphasized total penetration of the specimens and the attendant strength reductions were describable in terms of hole size.

We here attempt to present a rather basic description of how graphite-epoxy composites respond to laser radiation. Although we touch on cases of total penetration, we concentrate on the general cases where only partial penetration occurs. Using one material system, we investigate specimen thickness and stacking sequence effects using a wide range of incident beam intensities. For comparison we have investigated aluminum response under similar conditions. For examining load effects, we have irradiated coupons preloaded in tension. The induced damage is characterized in terms of residual tensile strength.

The following sections of this report detail objectives, approach, and the experimental and analytical results of the program. Section 2 - Technical Approach - deals with the program objectives and summarizes the tasks performed to fulfill these objectives. Section 3 - Thermal Characterization - details the thermal response and mass loss measurements during and after irradiation, provides the basic description of thermophysical damage mechanisms, and presents the models formulated to predict penetration susceptibility. Section 4 - Mechanical Characterization - presents all residual strength correlations for the laser-damaged coupons and compares these results with the control experiments and fracture-mechanics-based strength predictions. Section 5 - Conclusions and Recommendations - reiterates the salient results of the program and suggests additional areas of research.

2. TECHNICAL APPROACH

In this section we describe the approach used in this program to understand the response of graphite-epoxy materials to laser radiation. The program objectives are detailed, and the flow of tasks to accomplish these objectives follow.

2.1 PROGRAM OBJECTIVES

The overall goal of this program was to develop a basic understanding of the physical behavior of graphite-epoxy composite materials exposed to continuous-wave (CW) CO_2 laser radiation.

In order to achieve this goal, the following particular objectives were addressed:

- Compare the effects of laser radiation on graphite-epoxy laminates with those effects on aluminum, from the standpoint of (a) penetration vulnerability, and (b) strength degradation vulnerability.

- Determine penetration rate, thermal response and strength degradation of graphite-epoxy specimens exposed to CW laser beams.

- Identify the thermophysical mechanisms, other than complete penetration, involved in the laser-induced degradation of graphite composites.

- Formulate simple models to predict penetration rate and strength degradation in graphite composites exposed to CW CO_2 laser radiation.

These objectives were accomplished in a series of tasks which included specimen fabrication and baseline tensile strength characterization; testing of the specimens under various conditions of laser exposure and load; post-test characterization of laser damage by NDE techniques and residual strength tests; and formulation of models to predict the effects of laser damage in graphite-epoxy composites.

2.2 PROGRAM FLOW

Figure 2-1 summarizes the experimental and analytical investigations performed in the program. The paragraphs which follow provide particulars about these investigations and their interrelationships. Since the primary outputs of this program were to be thermal and mechanical characterization of laser-irradiated composites, detailed descriptions relating to these topics appear in Sections 3 and 4.

2.2.1 Specimen Fabrication and Control Experiments

Figure 2-2 summarizes the coupons used for these tests. The following 5208/T300 graphite-epoxy laminates were fabricated according to standard Fort Worth Division process specifications:

Thickness effects	$(0/\pm45)_S$	
	$(0/\pm45)_{4S}$	
Stacking Sequence effects	$(0/\pm45)_{2S}$	Longitudinal vs. transverse strength
	$(90/\pm45)_{2S}$	
	$(+45/90)_{2S}$	

The baseline laminate of the above set is the $(0/\pm45)_{2S}$, a 12-ply specimen of nominal thickness 0.073 in. (.185 cm).

For comparison purposes, a limited number of 2024(T81) aluminum specimens were used in the program. The aluminum thickness used (0.090 in.) was chosen to yield a specimen with approximately the same tensile capability as the baseline composite laminate.

All coupon specimens for laser testing were painted on one surface with a standard aircraft paint system of one coat epoxy primer and two coats urethane.

In addition to these "undamaged" specimens, 24 composite and 12 aluminum "notched" specimens were used for control experiments (described in Section 4). A total of 176 composite and 45 aluminum coupons were used for this program.

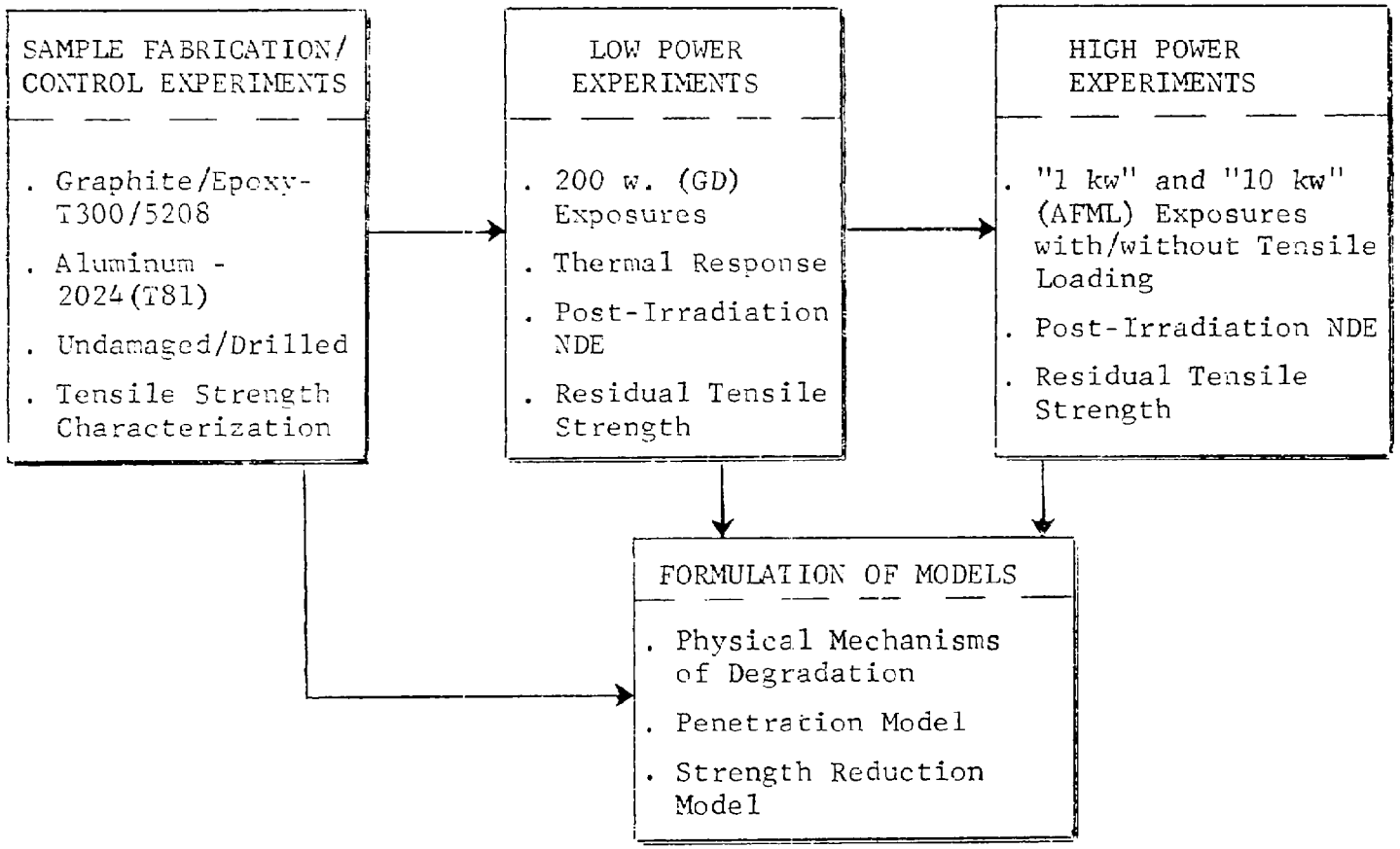

Figure 2-1 PROGRAM SUMMARY

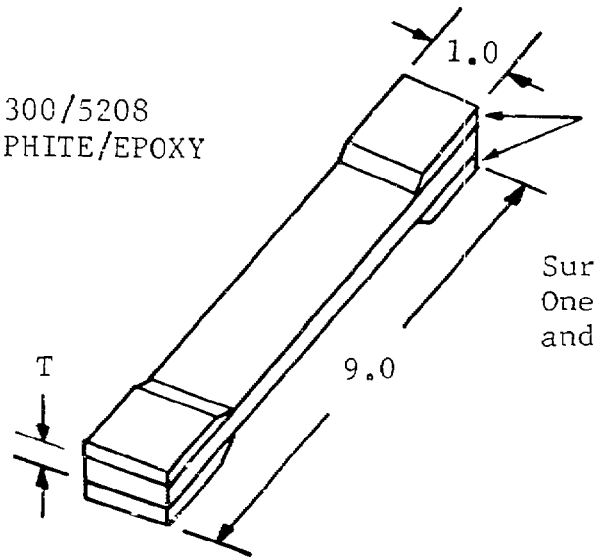

Surfaces Painted with
One Coat Epoxy Primer
and Two Coats Urethane

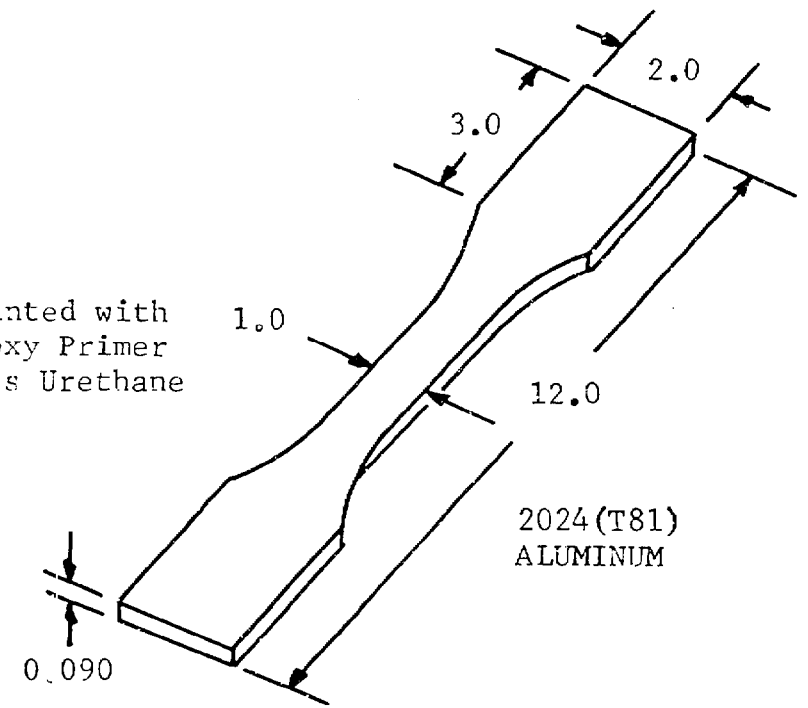

ASSEMBLY	LAMINATE	T*(PLIES)
-1	$(0/\pm45)_S$	6
-3	$(0/\pm45)_{2S}$	12
-5	$(\pm45/90)_{2S}$	12
-801	$(90/\pm45)_{2S}$	12
-803	$(0/\pm45)_{4S}$	24

*(Nominal Ply Thickness = 0.0055 in.)

Dimensions in inches

FIGURE 2-2 TEST COUPONS

A small number of additional composite specimens of the three thicknesses of the $(0/\pm45)_c$ class were used for thermal response measurements. These samples were 1 in. x 4 in. and 2 in. x 2 in.

A major premise of this program was that static residual strength is a useful measure of damage to composite materials and can be used to predict the life expectancy of a material subjected to a specific load history (Ref. 4). Indeed our previous work (Ref. 1) had indicated that laser-induced tensile strength degradation was characterizable in terms of circular hole strength reduction even without complete laser penetration of the specimens. It was thus important to obtain baseline information on control specimens, both undamaged and with controlled damage. Table 2-1 summarizes the control specimens which were failed in uniaxial tension to obtain this information. In Section 4, we will compare this baseline control information with common data reduction techniques used for analysis of the notched behavior of advanced composite laminates.

2.2.2 Low Power Laser Experiments

Table 2-2 summarizes the laser exposures of tensile coupons which were accomplished at General Dynamics. These irradiations were performed with a Model 41 Coherent Radiation Laboratory laser with incident beam power of 200 watts (essentially TEM_{oo} mode). Airflow was maintained parallel to the specimen surface (across the width) at approximately Mach 0.2, as measured by an Alnor Velometer. The temperature of each coupon was monitored with an iron-constantan thermocouple at various positions on the back surface.

The intent of these exposures was threefold, i.e., (1) to provide damage data at the low end of possible intensity scenarios; (2) to relate the present program results to earlier work on a different laminate (Ref. 1, 2), and (3) to obtain temperature distribution measurements.

In pursuance of (3) above, extensive additional temperature measurements were made on identical layup (but unpainted) laminates. These measurements monitored both front and back surface temperatures as a function of position and airflow. Discussion of these thermal response results appears in Section 3.

TABLE 2-1 CONTROL EXPERIMENTS*

Specimen Condition	$(0/\pm45)_S$	$(0/\pm45)_{2S}$	$(0/\pm45)_{4S}$	$(\pm45/90)_{2S}$	$(90/\pm45)_{2S}$	Aluminum
Unnotched	3+	3	3	3	3	3
0.125 in. dia. Drilled Hole-Through	3		3		3	3
0.125 in. dia. Drilled Hole-Half-Through			3			3
0.25 in. dia. Drilled Hole-Through	3		3		3	3
0.25 in. dia. Drilled Hole-Half-Through			3			3

*Ultimate Tensile Strength
+Number of Specimens
Total Composite Controls = 39
Total Aluminum Controls = 15

TABLE 2-2 LOW POWER EXPERIMENTS*

Power (Watts)	Beam Spot Size (cm^2)	Exposure Time (sec)	$(0/\pm45)_S$	$(0/\pm45)_{2S}$	$(0/\pm45)_{4S}$	$(\pm45/90)_{2S}$	$(90/\pm45)_{2S}$	Aluminum
200	0.2	5	3	3	3	3	3	3
200	0.2	10		3				
200	0.8	5	3	5	3	3	2	3
200	0.8	10					1	

* Notes:
1. Temperature measurement on each specimen
2. Airflow 0.2 M throughout
3. Post-Irradiation Measurements
   Mass Loss, X-ray, Residual Tensile Strength
4. General Dynamics Laser
5. Total Composite Coupons = 35; Total Aluminum = 6

It is worth noting at this point that little fiber damage is observed at these low incident powers. This is not to imply that these exposures are of no interest. Although most of the test coupons used have fiber-dominated tensile strengths, we will see in Section 4 that these low intensity exposures are rather effective at inducing strength reduction.

2.2.3 High Power Laser Experiments

Table 2-3 summarizes the laser exposures conducted at the Laser Hardened Materials Evaluation Laboratory of the AFML. In this compilation we have deleted those few specimens for which the experimental conditions (such as intermittent airflow) were not satisfactory. In Table 2-3a, the first series of AFML exposures at 750 watts incident power are detailed. The laser used for these experiments was a GTE Sylvania Model 971, which nominally operates single-mode, TEM_{00}. Approximately constant Mach 0.1 airflow was maintained across the width of the sample surface with a nozzle fed with compressed air.

The general plan for these exposures was to measure burnthrough times for selected specimens under given exposure conditions, and then produce "controlled depth" burns through approximately one-half and one-quarter of the thickness of the other specimens. Considering the $(0/\pm45)_{2S}$ baseline specimens for example, we attempted to penetrate successive numbers of the 0^{o} plies, since they contribute the major portion of the tensile strength capability. Much effort has been devoted to strength retention of notched specimens with through holes. This work intended to investigate the behavior of specimens in which definable amounts of partial penetration occurs. These results may then be compared with the partially through drilled control specimens for correlation with fracture models.

Tables 2-3b and 2-3c summarize the second series of exposures at the AFML. These experiments were performed with the 10 kilowatt "flat-top" laser, from which the beam intensity profile is essentially flat due to the large number of modes present. The specimens were positioned at the exit aperture of a subsonic wind tunnel for well-controlled and repeatable airflow across the specimen surface (width direction in all cases). In Table 2-3b we detail the experiments to produce controlled-depth burns, as in the 750-watt experiments. In order to predetermine

TABLE 2-3a HIGH POWER EXPERIMENTS - 0.75 kw

Power (kw)	Beam Spot Size (cm^2)	Exposure Time (Sec)	Comments	$(0/\pm45)_S$	$(0/\pm45)_{2S}$	$(0/\pm45)_{4S}$	$(\pm45/90)_{2S}$	$(90/\pm45)_{2S}$	Al
0.74-0.825	0.5	5.6-20.6	Burnthrough						4
0.75	0.5	3.0							1
0.75	0.5	5.0							3
0.75	0.5	10.6-11.2	Burnthrough	2					
0.75	0.5	25.5-25.7	Burnthrough		3				
0.75	0.5	12.8			3				
0.75	0.5	5.4		3					
0.75	0.5	2.7		2					
0.75	0.5	6.4			3	3	3	3	
0.75	0.5	12.8				3			
0.75	0.5	12.8	Unpainted Side			2			
0.75	0.2	1.3		3	3				

Notes:
1. Airflow 0.1 M throughout
2. 2 Aluminum and 3 Graphite-Epoxy Specimens not included - airflow problems
3. Post-Irradiation Measurements: Mass Loss, X-ray, Residual Strength
4. AFML Laser Facility
5. Total Composite Coupons = 37; Total Aluminum = 8

TABLE 2-3b HIGH POWER EXPERIMENTS - 5 and 10 kw

Power (kw)	Exposure Time (sec)	Comments	$(0/\pm45)_S$	$(0/\pm45)_{2S}$	$(0/\pm45)_{4S}$	$(\pm45/90)_{2S}$	$(90/\pm45)_{2S}$	Al
10	1.5				3			
10	0.8				3			
10	0.4				3			
10	0.8	Airflow 0.9M			3			
5	1.6			3				
5	0.8		3	3		3	3	
5	0.8	High Moisture Content		2			2	
5	0.4		3	3			3	3
5	0.2		3				3	3
5	0.7							3
5	0.4	Airflow 0.9M						2

Notes:
1. Airflow 0.3M except when noted.
2. Beam spot size 0.8 cm^2 throughout
3. Post-Irradiation Measurements: Mass loss, X-ray, Residual Strength
4. AFML Laser Facility
5. Total Composite Coupons = 46; Total Aluminum = 11

TABLE 2-3c HIGH POWER EXPERIMENTS - 5 kw WITH PRELOAD

Approx. Preload (fraction of undamaged ultimate strength)	Exposure Time (sec)	Failed or Survived	Comments	$(0/\pm45)_{2S}$	$(90/\pm45)_{2S}$	Al
	2.0	S		1		
	2.0	S	High Moisture Content	1		
	2.66	F		1		
0.3	2.54	F			1	
	2.77	F			1	
	2.0	F	Failed After Shot		1	
	1.0	F	Failed After Shot		1	
0.4	1.6	F			1	
	0.4	S				1
	0.49	F				1
	0.56	F				1
	1.67	F	High Moisture Content	1		
0.5	0.17	F		1		
	1.0	F	Failed After Shot	1		
	0.8	S		1		
	0.2	S		1		
0.7	0.5	F	Failed After Shot	1		
	0.83	F		1		

Notes:
1. Incident Power - 5 kw, Beam Spot Size 1.23 cm^2, Airflow 0.3M
2. Post-Irradiation Measurements on Survivors: Mass Loss, X-ray, Residual Tensile Strength
3. AFML Laser Facility
4. Total Composite Coupons = 15; Total Aluminum = 3

the exposure times for these shots, a small group of exposures at 5 and 10 kw were performed on 1 x 4 in. laminates and aluminum for accurate burnthrough time measurements.

Table 2-3c lists the exposures of specimens loaded in tension to various fractions of their undamaged strength. A Tinius-Olsen test machine was positioned so that the preloaded specimen was located approximately at the center of the wind tunnel exit. The airflow conditions in this case were thus somewhat different in that both front and back surfaces were in the airflow; in all other cases (without load) air flowed only across the front surface of the samples. These preloaded specimens were irradiated until fracture or burnthrough, whichever occurred first, or in some cases for a preset time during which neither burnthrough nor fracture occurred.

2.2.4 Post-Test Characterization

After laser testing, all survivors were evaluated with two types of measurement: (1) physical extent of damage, and (2) residual tensile strength.

With regard to (1), the following measurements were performed on the irradiated graphite-epoxy specimens: mass loss, visual (low power microscope) measurement of "hole" size, conventional X-ray, and X-ray with a radiopaque additive, tetrabromoethane (TBE). The mass loss gives a quantitative description of the amount of material lost from the specimen, but it is also necessary to measure the areal extent of damage. Essentially all the specimens considered here were only partially penetrated. The damage thus consists of regions of removed fiber and resin, missing resin only, and "heat-effected" zones where, for example, the resin may be heated, melted, partially decomposed, and resolidified.

Where applicable, we measured the ply-by-ply dimensions of removed fiber zones under low-power magnification. Conventional X-ray also yields this information about the profile of removed material, but neither measurement may adequately indicate the extent of the heat-affected area. The TBE-enhanced X-rays should yield information about such damage, since the TBE enters the void/crack areas by capillary action. These enhanced X-rays thus measure a damage area larger than that indicated by visual or conventional X-ray, since subtle areas of missing or damaged epoxy may be detected.

In combination then, these measurements contain the elements required to thoroughly characterize the physical extent of the damage, i.e., the volume of material removed, the size of the zone of removed material and "heat-affected" material, and (by inference) the "effective" depth of the burn.

After this characterization of the damage zone was complete, each specimen was tested for residual tensile strength. As noted earlier we know that static residual strength is a useful measure of damage to composite materials and can be used to predict the life expectancy of the material subjected to a specified load history. By thus having this damage size and residual strength characterization, we are able to describe the strength degradation as a function of laser exposure (Section 4).

Although the residual strengths were also measured for the aluminum coupons, minimal attention was devoted to physical damage characterization of these specimens. Mass loss was measured in each case, but further description of the damage zone is quite difficult. Since few aluminum coupons were penetrated, the "hole" was a somewhat vaguely defined crater surrounded by melted and resolidified material, with the extent and shape of such regions strongly varying from shot to shot.

2.2.5 Model Formulation

The intent of this task was to formulate models which would (1) identify and correlate the physical mechanisms contributing to the thermal degradation of laser-irradiated advanced composite materials; (2) predict the penetration vulnerability (3) the strength degradation vulnerability of these materials.

Using the measured thermal response and mass losses, we have provided a description of how laser radiation interacts with graphite-epoxy materials and a model to predict mass ablation and penetration time. These features are discussed in detail in Section 3.

Using the measured damage and residual strength characterization, we have correlated the strength degradation with damage parameters and laser exposure parameters, and have provided a model framework with which to predict laser-induced strength degradation using familiar fracture concepts. Details of the mechanical characterization and modeling appear in Section 4.

3. THERMAL CHARACTERIZATION

In this section we describe how a laser beam interacts with graphite/epoxy composite material. We provide both a qualitative and quantitative description of this interaction by addressing the physical mechanisms which determine time-dependent temperature distribution, mass ablation and penetration rate. For the case of high beam intensities we apply the same general description of mass ablation and penetration rate to aluminum.

The situation treated here is unquestionably complex, for in the case of composites we deal with a non-isotropic, inhomogeneous system in which the two constituent materials may experience some combination of damage mechanisms which include anaerobic charring processes, oxidation, melting and sublimation. We will see, however, that the thermal degradation is characterizable and reasonably predictable for the conditions investigated.

In the following discussions the specimen thickness is designated by δ (cm), the laser power by P(w), the beam radius, as measured by ablation of plexiglass, by r(cm), and the beam intensity (or power density) is defined by

$$I = P/\pi r^2 \qquad (3\text{-}1)$$

Exposure times are designated by t_e(sec), burnthrough times by t_b(sec) and mass loss by Δm(gm).

3.1 EXPERIMENTAL MEASUREMENTS

Measurements were made of temperature rise, burn area, non-burnthrough mass loss, and, in the case of some of the high power experiments, burnthrough time. Representative data for 5208/T300 composite and, in a relatively few cases, aluminum are shown in the figures and tables cited below. These data have been selected to illustrate the observable features that must be accounted for by a comprehensive model

of laser-induced heating, mass-ablation and penetration. Although some results have been omitted in the interest of concise presentation, the data shown for cases in which more than one run was made under the same conditions are typical in regard to experimental scatter.

Temperatures during and after the laser exposure at 200 watts incident power were determined by means of thermocouples attached on the front or back surface of the exposed specimen. The most significant responses are considered to be those measured on the beam axis directly behind the burn area. Off-axis responses also were measured on the front and back of some specimens at distances of 1 or 2 spot radii from the beam axis. Typical back surface temperature responses are shown in Figure 3-1. The symbols C, D, and U refer respectively to cases where the thermocouple was on the axis, at a point downstream relative to the wind, and at a point upstream relative to the wind. In these cases the specimens were $(0/\pm 45)_{2S}$ laminates. Figure 3-1 shows a significant feature which is typical of on-axis back surface temperature responses for a laser power of 200 watts, namely, that there is little difference between the responses for beam-spot radii of $r = 0.25$ cm and $r = 0.50$ cm. This result is consistent with the assumption that, for beam intensities of about 1100 watts/cm^2 or less, the exposed composite surface rapidly comes to a steady state temperature which is independent of beam spot size and which extends over a radius which is large compared to the specimen thickness.

Burn areas were characterized either by visual inspection or by the enhanced X-ray method using TBE penetrant. Typical surface burn areas for unpainted composite specimens are sketched in Figure 3-2. The primary burn areas, designated as A', were visually identifiable by a distinct perimeter within which the composite surface, viewed normally, has a glossy, almost metallic appearance. In some cases a small crater appears near the center of the burn area. In all cases a "tail" of discoloration on an apparently intact surface appears on the leeward side of the burn area. When similarly exposed specimens were sectioned through the center of the burn area by sawing, it was found that the three-dimensional damage region due to low intensity irradiation is approximately a parabola of revolution about the beam axis within which the residual composite material is jet black (if not removed).

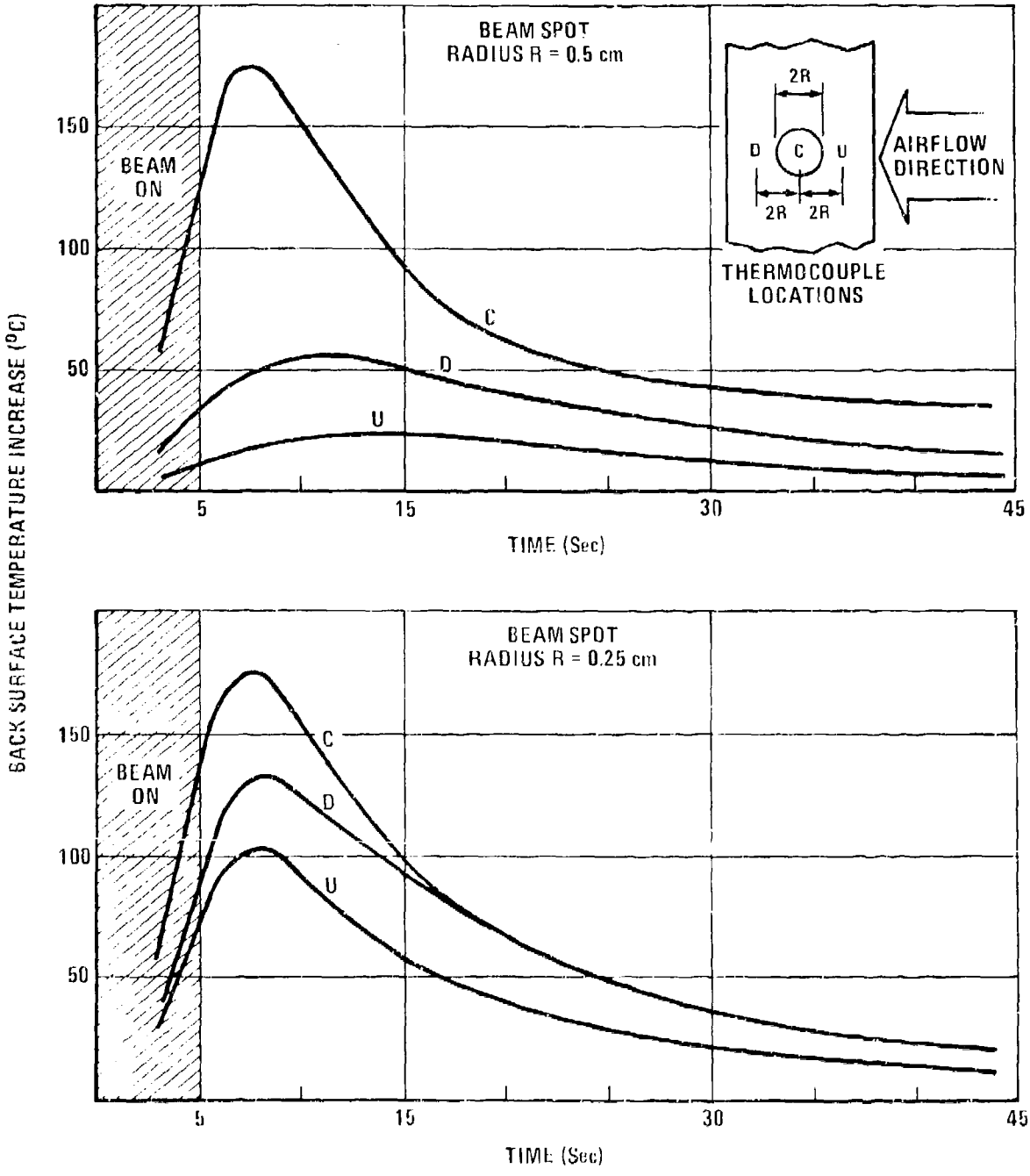

Figure 3-1 Effect of Airflow and Spot Size on Back Surface Temperature – 200 Watt Beam

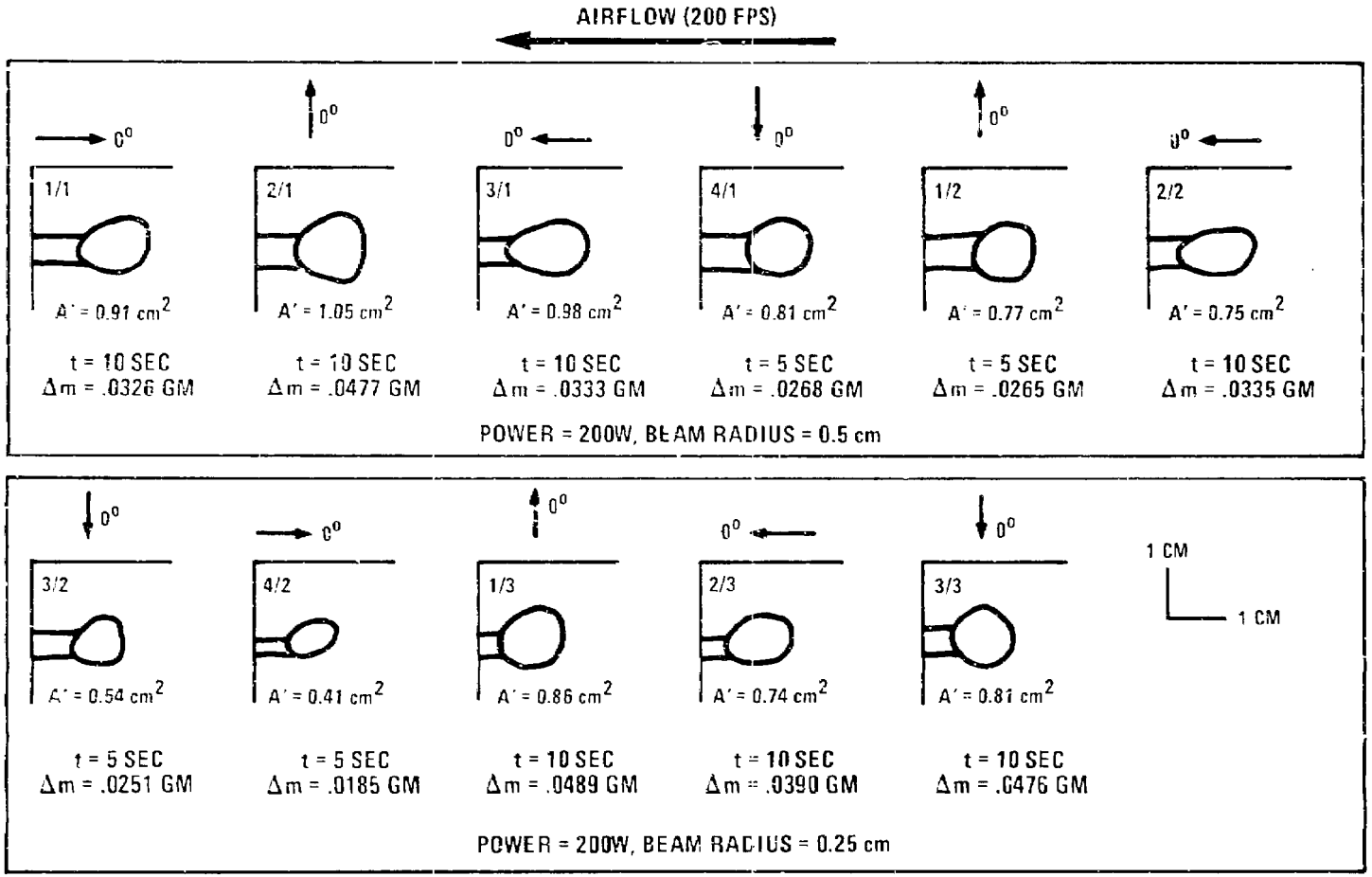

Figure 3-2 Surface Damage Pattern from Low Power Irradiation of $(0/\pm45)_{4s}$ Laminates

This region appears to consist of fibers depleted of resin. A significant feature of the surface burn areas shown in Figure 3-2, and also apparent in the enhanced X-ray inspection of painted specimens, is that the burn area A' is not much bigger for a beam spot radius of r = 0.5 cm than for a beam spot radius of r = 0.25 cm. This observation supports the assumption suggested by on-axis temperature rise, namely, that the temperature of the exposed surface is roughly independent of beam spot size for intensities of 1100 watts/cm^2 or less.

Non-burnthrough composite mass losses for a number of powers and spot sizes are given in Table 3-1. Similar data for non-burnthrough shots on aluminum are given in Table 3-2. A significant feature of the composite irradiations at 200 watts is that for a given thickness and exposure time the mass loss is approximately independent of beam-spot size. This observation complements the conclusions based on measurements of on-axis back-surface temperature rise and surface burn-area cited above. The 200 watt data, taken together, are consistent with the assumption that, for intensities less than or equal to about 1100 watts/cm^2, mass is sublimated at constant temperature from an area which is independent of beam spot size and at a rate per unit area which also is independent of beam spot size. However, the 200 watt mass losses as a function of exposure time for either spot size suggest that the mass lost is not strictly proportional to exposure time; rather the rate of mass-loss increases with increasing exposure time. A tendency toward increasing mass loss with decreasing specimen thickness is also apparent. All of these features of the low intensity data are explained by a model proposed below. On the other hand, Figure 3-3 shows that at higher intensities (750 watts, 0.4 cm spot radius) the mass loss is proportional to time and only weakly dependent on specimen thickness.

Data on times required for complete burnthrough of composite and aluminum specimens are given in Table 3-3. In accord with the non-burnthrough 750 watt data on composites shown in Table 3-1 and Figure 3-3, it is seen that the burnthrough time at a given power and beam-spot size is approximately proportional to specimen thickness. Furthermore, the time required to penetrate a 24-ply specimen at an intensity of 12,700 watts/cm^2 is approximately equal to the time required

Table 3-1 Measured Mass Loss in Non-Burnthrough Shots on Composites

No. Spec.	Airflow (M)	Laminate	δ(cm)	P(w)	r(cm)	T_e(sec)	Δm(gm)
3	0.2	$(0/\overline{+}45)_S$	0.094	200	0.25	5	0.051±.002
3	"	"	"	"	0.50	5	0.052±.001
3	0.2	$(0/\overline{+}45)_{2S}$	0.185	200	0.25	10	0.102±.001
3	"	"	"	"	0.25	5	0.045±.002
5	"	"	"	"	0.50	5	0.043±.002
3	0.2	$(0/\overline{+}45)_{4S}$	0.343	200	0.25	5	0.041±.001
3	"	"	"	"	0.50	5	0.033±.001
3	0.1	$(0/\overline{+}45)_S$	0.094	750	0.40	5.4	0.123±.005
2	"	"	"	"	0.40	2.7	0.075±.001
3	"	"	"	"	0.25	1.34	0.033±.002
3	0.1	$(0/\overline{+}45)_{2S}$	0.185	750	0.40	12.8	0.257±.003
3	"	"	"	740	0.40	6.4	0.137±.010
3	"	"	"	750	0.25	1.34	0.018±.001
3	0.1	$(0/\overline{+}45)_{4S}$	0.343	750	0.40	12.8	0.232±.009
3	"	"	"	"	0.40	6.4	0.108±.001
2*	"	"	"	"	0.40	12.8	0.208±.002
3	0.3	$(0/\overline{+}45)_{4S}$	0.343	10000	0.50	1.5	0.495±.002
3	"	"	"	"	0.50	0.8	0.249±.001
3	"	"	"	"	0.50	0.4	0.124±.001
3	0.9	"	"	"	0.50	0.8	0.237±.001
**1	0.3	$(0/\overline{+}45)_S$	0.094	10000	1.74	2.0	0.73

δ (cm) = specimen thickness; P(w) = laser power; r(cm) = spot radius

t_e(sec) = exposure time; Δm(gm) = measured mass loss

*Unpainted specimens; all others painted
**Data point from Ref. 14

Table 3-2 Measured Mass Loss in Non-Burnthrough Shots on Aluminum*

No. Spec.	Airflow (M)	δ(cm)	P(w)	r(cm)	t_e(sec)	Δm(gm)
3	0.2	0.230	200	0.25	5	0.003±.001
3	"	"	"	0.50	5	0.002±.001
1	0.1	0.230	740	0.40	10	0.050
3	0.1	0.230	750	0.40	5	0.050±0.030
1	0.1	0.230	750	0.40	3	0.013
3	0.3	0.230	5000	0.50	0.7	0.144±.060
3	"	"	"	0.50	0.4	0.091±.020
3	"	"	"	0.50	0.2	0.045±.003
1+	"	"	"	0.625	0.4	0.185

δ(cm) = specimen thickness; P(w) = laser power, r(cm) = spot radius

t_e(sec) = exposure time; Δm(gm) = measured mass loss

*All specimens painted
+Specimen preloaded at 2800 lbs during exposure

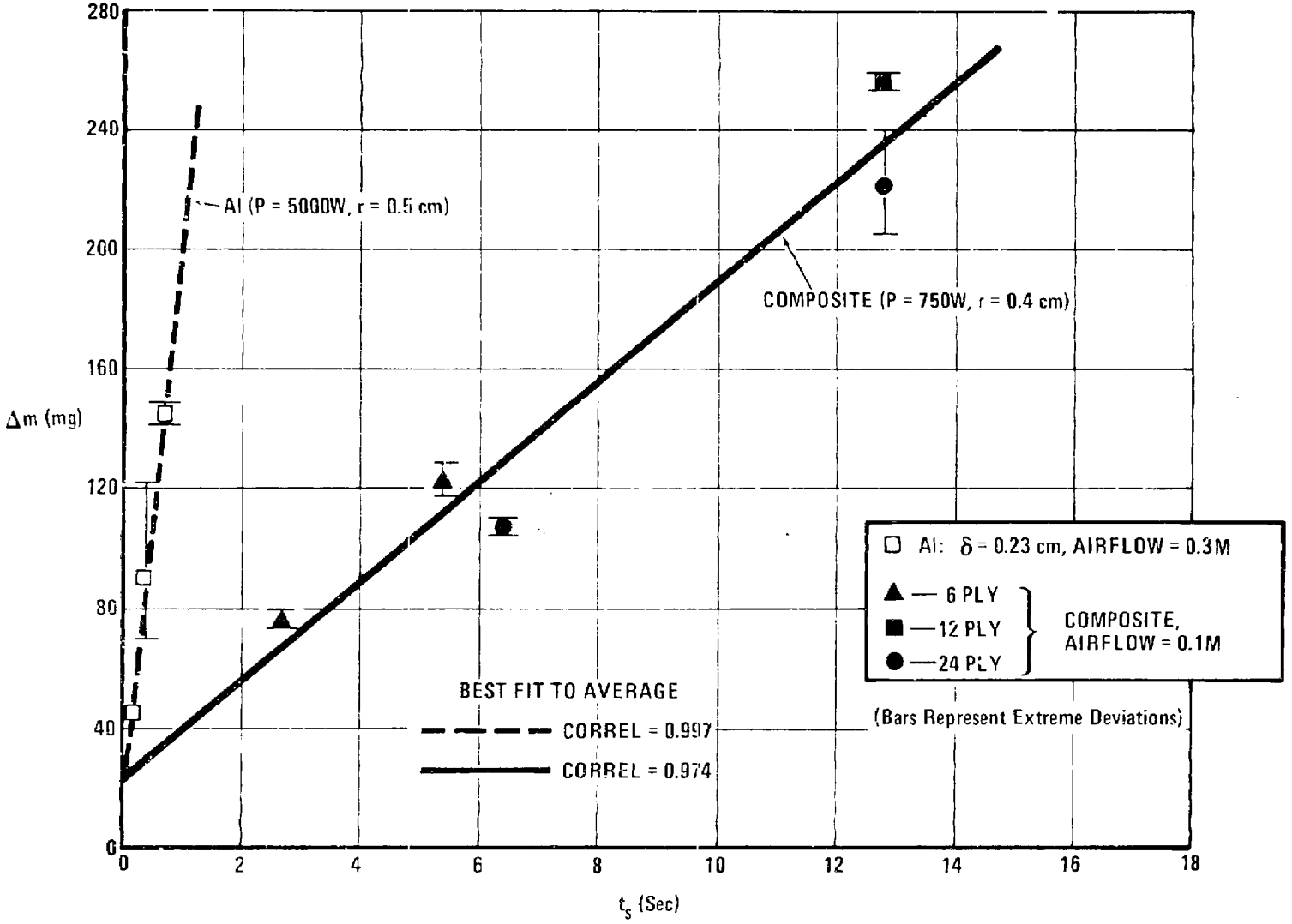

Figure 3-3 Mass Loss vs Exposure Time for Aluminum and Composites

Table 3-3 Measured Burnthrough Times
for Composites and Aluminum

No. Spec.	Airflow (M)	Laminate	δ(cm)	P(w)	r(cm)	I(w/cm^2)	t_b(sec)	Δm(gm)
1	0.2	$(0/\overline{+}45)_S$	0.091	750	0.4	1500	10.56	0.211
1	"	"	0.094	750	0.4	1500	11.22	0.211
1	0.2	$(0/\overline{+}45)_{2S}$	0.179	750	0.4	1500	25.65	0.412
1	"	"	0.182	750	0.4	1500	25.57	0.420
1	"	"	0.176	750	0.4	1500	25.53	0.417
1*	0.2	$(0/\overline{+}45)_{2S}$	0.170	10000	0.5	12700	0.80	0.332
1*	0.2	$(0/\overline{+}45)_{4S}$	0.338	10000	0.5	12700	1.63	0.649
1*	0.2	$(0/\overline{+}45)_{2S}$	0.170	5000	0.5	6400	1.88	0.301
1	0.2	(Al)	0.23	10000	0.5	12700	0.5	-
1	0.2	(Al)	0.23	5000	0.5	6400	0.8	-

δ(cm) = specimen thickness; P(w) = laser power; r(cm) = spot radius

t_e(sec) = burnthrough time

*Unpainted specimens

to penetrate a 12-ply specimen at half that intensity. This means that for intensities of 6400 w/cm^2 or higher the rate of penetration is proportional to intensity. This proportionality does not extend to intensities at low as 1500 w/cm^2. Data on mass loss in the burnthrough shots, included in Table 3-3 and converted to effective volumes by assuming a composite density of 1.569 gm/cm^3, show that the through-holes have an effective radius which is only about 25% higher than the nominal beam radius at the higher intensities, but have an effective radius appreciably larger than the nominal spot radius for an intensity of 1500 w/cm^2. Data from the two aluminum penetrations suggest that the proportionality between penetration rate and beam intensity also applies to aluminum at intensities about 6400 w/cm^2.

Thus, it is seen that the data on composites can be divided into three groups on the basis of beam intensity. Inasmuch as the exact demarcations of the three intensity ranges cannot be determined from the available data, we designate the upper bound of the lowest intensity range by I_L and the lower bound of the highest intensity range by I_H. Laser interactions with composites then can be characterized as follows.

Low Intensity Range: $I < I_L$ ($1100 < I_L < 1500$ w/cm^2)

Mass loss rate is proportional to power, is independent of spot size (intensity), and increases with increasing exposure time and decreasing specimen thickness; on-axis back-surface temperature rise, damage area and mass loss suggest mass ablation occurs at constant temperature and constant rate per unit area; exposures less than 10 sec mainly remove resin, not fiber.

Intermediate Intensity Range: $I_L \leq I \leq I_H$ ($1500 < I_H < 6400$ w/cm^2)

Both fibers and resin are removed; penetration and mass loss are proportional to exposure time and approximately independent of specimen thickness, but effective burn radius is substantially larger than nominal beam radius.

High Intensity Range: $I_H < I$

Fibers and resin are removed as in a drilling process; penetration and mass loss are proportional to exposure time and independent of specimen thickness; effective burn radius is not much greater than nominal beam radius; penetration rate is proportional to beam intensity; in this intensity range aluminum response is similar to that of composites.

3.2 QUALITATIVE DESCRIPTION OF LASER INTERACTION WITH COMPOSITES

On the basis of the experimental results and direct inferences cited in Section 3.1, we propose the following qualitative model for laser interaction with composites. For specificity and for use in the subsequent quantitative formulation we introduce relevant symbols in this section.

Low Intensity Range: $I < I_L$ $(1100 < I_L < 1500\ w/cm^2)$

The absorptivity of 10.6 μm radiation on the specimens is near unity. Convective cooling and radiative emission are negligible at the temperatures involved. The laser beam rapidly burns away paint and any resin lying within the beam spot and over the fibers of the outer ply. The fibers of the outer ply then start to heat, a large fraction $(1 - \eta_1)$ of the absorbed power P(w) being taken up by local fiber heating and thermal conduction along the length of the fibers (transverse to the beam). Only a relatively small fraction η_1 of the absorbed laser power is transferred to the resin. However, this transfer commences, almost immediately, when the exposed fibers near the center of the beam spot reach a temperature T_M at which the resin decomposes and sublimates at normal pressure. As the exposure continues, the radius within which the fiber temperature exceeds T_M progressively expands to larger values at a rate which is sensitive to the thermal conductivity of the fibers along their length but insensitive to the beam spot size.

The resin decomposes and sublimates at a constant mass rate per unit area γ (gm/cm^{2}sec) over an area A' (t_e) located just behind the outer fibers. The resin sublimation area A'(t_e) expands as a function of exposure times t_e but is always smaller than the outer fiber area over which the temperature exceeds the resin decomposition temperature T_M. Its actual size at a given time is determined by the requirement that the incident power into the resin, $\eta_1 P$, must be balanced by (1) one-dimensional conduction and heating of the composite material along the beam axis, which is given by A' and the following parameters of the specimen: thermal conductivity of the composite normal to its plies. κ (watts/cm$^\circ$C), density, ρ (gm/cm^3), specific heat, C_p(J/gm$^\circ$C) and specimen thickness, δ (cm); and (2) heat required for resin decomposition and sublimation, given by A', sublimation rate per unit area, γ, and a heat of decomposition and sublimation, L_1(J/gm). In the case of 5208 resin, the decomposition and sublimation heat L_1 corresponds to reversion of the cured resin to its TGMDA and DDS monomers or closely related products.

Intermediate Intensity Range: $I_L < I < I_H$ ($1500 < I_H < 6400$ w/cm^2)

If the beam intensity exceeds I_L, the temperature of the outer fibers in the vicinity of the beam spot soon reaches a point where a runaway effect occurs because of decreasing thermal conductivity with increasing temperature. As the fibers are heated locally, the thermal conductivity along the fiber length drops and favors an even higher local temperature. This situation limits the growth of the resin sublimation area A' and leads to sublimation of the graphite fibers. When the fibers are burned through, the process re-commences on the next ply. The effective burn radius will be appreciably larger than the beam spot because of the growth of A' prior to fiber sublimation. In this range radiative emission is important.

High Intensity Range: $I_H < I$ $(1500 < I_H < 6400\ w/cm^2)$

In this intensity range the runaway effect described above occurs so rapidly that the graphite fibers are sublimated only over the area of the beam spot, within which graphite and resin are removed in proportion to their concentrations in the composite as a whole. The mass ablation rate per unit area, $\dot{\mu}$ (gm/cm^2 sec), is proportional to intensity I(w/cm^2) and is determined by factors relating to the effusion of monatomic, diatomic and triatomic carbon from a graphite surface at temperature T(^{o}K). The heat required to decompose and sublimate the resin is negligible, but the rate of mass loss per unit area depends on the resin mass fraction (1-f), f being the mass fraction of the non-polymeric component (graphite).

The rate per unit area at which C, C_2 and C_3 molecules effuse from the exposed graphite fibers is related to beam intensity through an energy balance involving an effective heat of ablation L_2(J/gm), and a mass effusion rate characteristic of graphite sublimation at temperature T(^{o}K). Sublimated carbon molecules are removed from the vicinity of the graphite surfaces by convection and chemical reaction in air so rapidly that the rate of effusion approaches that in a vacuum. Carbon sublimation therefore is characterized by an effective equilibrium vapor pressure $p_e(T)$, an accommodation coefficient (or sticking probability) α and effective molecular mass M. The temperature dependence of the effective vapor pressure $p_e(T)$ is characterized by a hypothetical vapor pressure at infinite temperature p_∞ (dyne/cm^2) and an Arrhenius-type activation energy L' (cal/mole).

Energy loss due to radiative emission, though high from the standpoint of detectability, is negligible compared to energy absorbed in sublimation in this energy range, since the former increases only as fourth power of absolute temperature, whereas the latter increases exponentially as an inverse absolute temperature. The laser power absorbed by heating and sublimation of the graphite fibers is proportional to the rate of effusion and to the heat of ablation L_2(J/gm). The latter consists of L_S(J/gm), the heat of sublimation of graphite, and a relatively small contribution ΔH(J/gm) which represents the energy required to raise the graphite to temperature T(^{o}K). At somewhat lower beam intensities radiative emission becomes

important in the energy balance, its magnitude being determined by an emissivity ϵ and the Stefan-Boltzmann constant σ. The emissivity ϵ and the absorptivity η are both near unity for composites.

Mass ablation of aluminum in the high intensity range is qualitatively similar to that for composites. In this case the non-polymeric mass fraction is $f = 1$. Aluminum atoms sublimate from molten metal for which the absorptivity η and emissivity ϵ are near unity, as in the case of graphite.

3.3 COMPOSITE TEMPERATURE CORRELATIONS AT LOW BEAM INTENSITY

In this section we show that the qualitative description of low-intensity interactions described in Section 3.2 implies a quantitative formulation which provides a good description of temperature response on the back surface of an exposed composite specimen as measured by a thermocouple located directly behind the beam spot. It therefore can be assumed that the formalism, together with the inferred parameters, yields the time-dependent temperature distribution inside the composite material along the laser beam axis. From this time-dependent distribution one can calculate, for example, temperature gradients which determine interlaminar normal thermal-stresses.

We regard the specimen as a slab whose temperature is initially uniform. When the laser exposure starts, the surface directly behind the outer fibers comes to a temperature T_M at which the resin decomposes and sublimates. If we assume that (a) the radius of the area A' over which the resin is at temperature T_M is much larger than the specimen thickness, (b) the exposure times considered are small enough that the thickness of intact resin along the beam axis is not appreciably decreased, and (c) heat transfer from the back surface is negligible, then the time-dependent temperature along the beam axis is obtained by solving a simple slab problem.

We define

t_e(sec) = time after onset of heating (i.e., exposure time)

δ(cm) = slab thickness

z(cm) = distance inside slab (measured from hot surface)

T_o(^oC) = initial slab temperature (assumed to be 20^oC)

T_M(^oC) = temperature at hot surface

T(^oC) = temperature at time t_e, depth z

ρ(gm/cm^3) = slab density

C_p(J/gm^oC) = specific heat

κ(watts/cm^oC) = thermal conductivity

If the face at $z = \delta$ is kept insulated, the problem of finding $T(z,t_e)$ is stated mathematically as follows:

$$\kappa \frac{\partial^2 T}{\partial z^2} - \rho C_p \frac{\partial T}{\partial t_e} = 0 \qquad (0 < z < \delta \ , \ t_e > 0) \tag{3-2}$$

$$T(+0, t_e) = T_M \qquad (t_e > 0) \tag{3-3}$$

$$\kappa \left(\frac{\partial T}{\partial z}\right)_{z=\delta} = 0 \qquad (t_e > 0) \tag{3-4}$$

$$T(z, +0) = T_o \qquad (0 < z < \delta) \tag{3-5}$$

The solution of the above boundary-value problem is

$$T-T_o = (T_M-T_o)\left\{1 - \frac{2}{\pi}\sum_{n=1}^{\infty}(n-\tfrac{1}{2})^{-1}\exp\left|-(n-\tfrac{1}{2})^2 kt_e\right|\sin(n-\tfrac{1}{2})x\right\} \quad (3\text{-}6)$$

for $(0 \leq z \leq \delta,\ t_e > 0)$ where

$$x \equiv \pi z/\delta \quad (3\text{-}7)$$

and

$$k = \pi^2 \kappa /\rho C_p \delta^2 \quad (3\text{-}8)$$

If the heat input is stopped at time t_e and both faces are assumed to be insulated thereafter, then solution of a similar boundary-value problem with the above expression for $(T-T_o)$ as an initial condition shows that the temperature at a later time t (measured from the same starting point as t_e) is given by

$$T-T_o = (T_M-T_o)\left\{1 - \frac{2}{\pi^2}\sum_{n=1}^{\infty}(n-\tfrac{1}{2})^{-2}\exp\left|-(n-\tfrac{1}{2})^2 kt_e\right|\right. \quad (3\text{-}9)$$

$$- \frac{4}{\pi^2}\sum_{j=1}^{\infty}\sum_{n=1}^{\infty}\left|(n-\tfrac{1}{2})^2 - j^2\right|^{-1}\exp\left|-(n-\tfrac{1}{2})^2 kt_e\right|$$

$$\left.\exp\left|-j^2 k(t-t_e)\right|\cos jx\right\}$$

where x and k have the definitions given above.

If the parameters T_M, ρ, C_p and κ are known, the temperature rise at the back surface of an exposed composite specimen at time t_e during the irradiation can be obtained by setting $x = \pi$ in Equation (3-6). Similarly, the back surface temperature at a time $(t-t_e)$ after the beam has been turned off can be calculated by substituting $x = \pi$ in Equation (3-9). We have used measured values of ρ, C_p and κ, together with a value of T_M obtained by applying Equation (3-6) to a single back-surface temperature measurement, to predict the back-surface temperature rise as a function of time for three different specimen thicknesses.

The density of the composite material used in our experiments is

$$\rho = 1.569 \text{ gm/cm}^3 .$$

The specific heat C_p and the thermal conductivity at right angles to the plies, κ, both increase as a function of temperature, but data obtained by Reynolds and Weltman at this facility show that in the vicinity of 300°C they approach the nominal values

$$C_p = 1.214 \text{ J/gm}^\circ\text{C}$$

$$\kappa = 0.00383 \text{ watts/cm}^\circ\text{C} .$$

Substituting these values into Equation (3-8) we obtain the following inverse time constants for the three specimen thicknesses considered:

$$\text{6-ply } (\delta = 0.094 \text{ cm}) : k = 2.25 \text{ sec}^{-1}$$

$$\text{12-ply } (\delta = 0.185 \text{ cm}) : k = 0.580 \text{ sec}^{-1}$$

$$\text{24-ply } (\delta = 0.343 \text{ cm}) : k = 0.169 \text{ sec}^{-1}$$

We have estimated T_M from the measured temperature rise at the back surface of a 12-ply specimen after 4.5 sec of exposure to a 200 watt beam with a spot radius of 0.5 cm. The rise was 112°C. Substituting $x = \pi$, $k = 0.580$ sec^{-1}, $t_e = 4.5$ sec and $T-T_o = 112°C$ into Equation (3-6), we obtain

$$T_M - T_o = 330°C \ .$$

Taking the initial specimen temperature to be $T_o = 20°C$, we conclude that 5208 resin decomposes and sublimates at about

$$T_M = 350°C \ .$$

Substituting the above values of T_M, ρ, C_p and κ into Equations (3-6) and (3-9) with $x = \pi$, we have made predictions of the back surface temperature rises as a function of time (t_e or t) after onset of beam. The predicted temperature response curves for three different specimen thicknesses are compared with experimental data in Figure 3-4. It is seen that the overall agreement is satisfactory for measurements taken on the 12- and 24-ply specimens during and slightly after the irradiation. The 6-ply predictions are only correct to the right order of magnitude. However, these results could be brought into much better agreement by shifting the experimental exposure times downward by about 0.3 sec, which was in fact the approximate uncertainty in the exposure time measurements.

It should be noted that the model which has been used rather successfully to correlate back surface temperature rise does not involve either power or intensity. Its limits of applicability extend only to powers high enough to produce prompt resin sublimation and low enough that fiber sublimation is not important. However, the assumption that it applies to powers substantially higher and lower than 200 watts seems to be warranted by the fact that the predictions are equally good for the two spot radii employed.

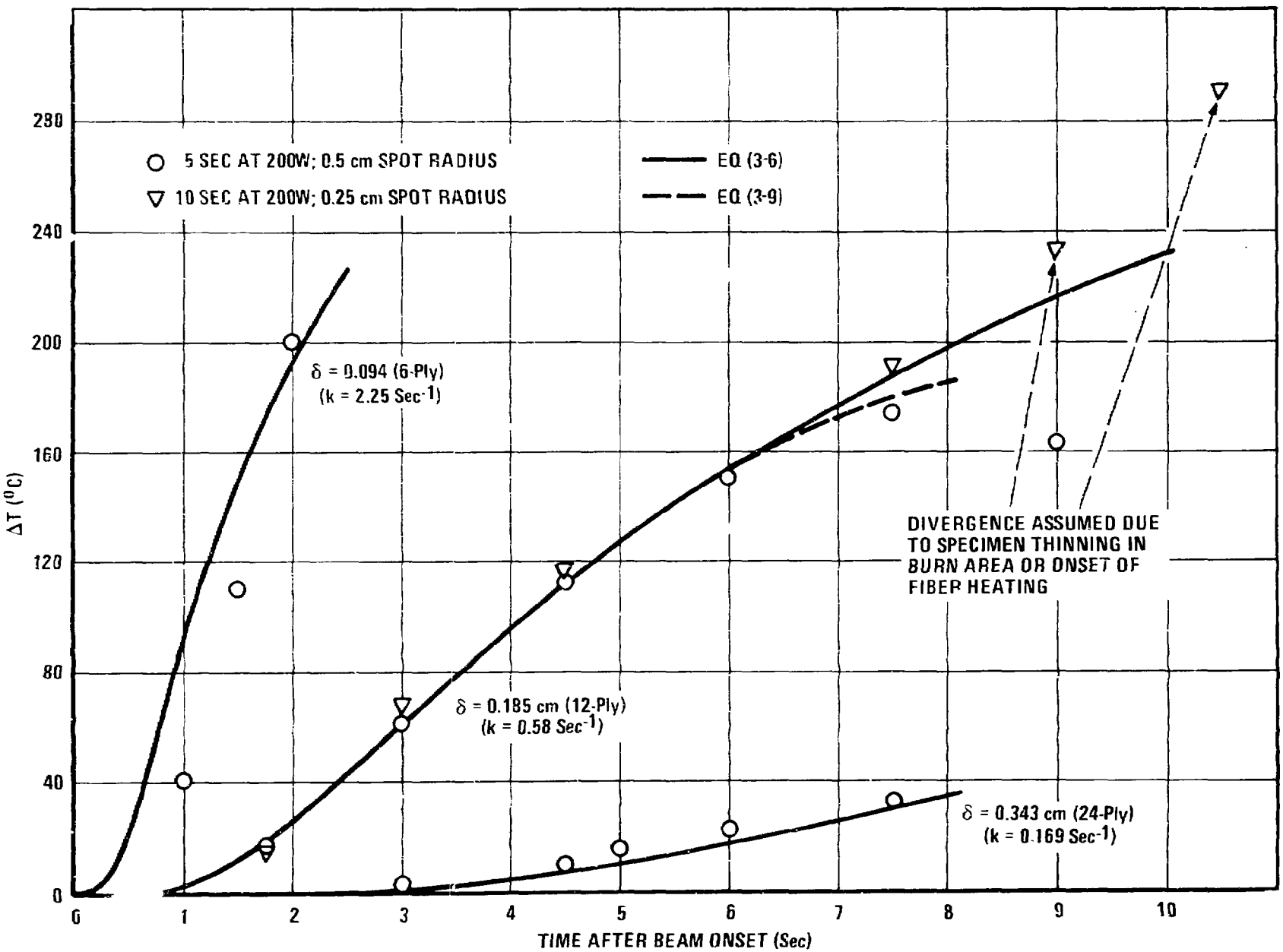

Figure 3-4 Temperature Rise Behind Beam Spot for $(0/\pm45)_c$ Composites

The temperature response analysis performed above has yielded a value for the resin decomposition temperature T_M and established independent support for the measured values of ρ, C_p and κ. All four of these parameters can now be used in the following section on mass loss at low beam intensity. Direct use will be made of the temperature distribution given by Equation (3-6).

During thermal expansion tests performed in our Engineering Chemistry Laboratory, it has been noted that 5208 resin starts emitting smoke at about 625°F (329°C) and undergoes complete mechanical collapse at slightly higher temperatures. This effect is reasonably consistent with our derived resin decomposition temperature of $T_M = 350°C$.

3.4 COMPOSITE MASS LOSS AT LOW BEAM INTENSITY

A qualitative description of mass loss at low beam intensity, and an enumeration of the parameters involved, is given in Section 3.2. The corresponding quantitative formulation developed here accounts reasonably well for the observed mass losses as a function of exposure time and specimen thickness. It also appears to predict the size of the burn area on the exposed surface. In effect then, our quantitative model provides a description of the region over which matrix material is removed. The dimensions of this region are significant from the mechanical standpoint, since, even if the graphite fibers remain intact, the tensile and particularly the compressive strength of the composite depends upon the presence of resin.

The qualitative description of low intensity mass ablation given in Section 3.2 can be expressed quantitatively as follows. The rate at which resin mass is sublimated from the exposed surface is given in terms of the specimen mass m and the exposure time t_e by

$$\frac{dm}{dt_e} = -\gamma A'(t_e), \qquad (3\text{-}10)$$

where γ (gm/cm^2 sec) is a constant and where A'(cm^2) is an expanding area just behind the fibers of the outer ply. The

size of A' at a given time t_e is determined by the energy balance

$$\eta_1 P = L_1 \gamma A'(t_e) - A'(t_e) \kappa \left(\frac{\partial T}{\partial z}\right)_{z=0} , \qquad (3\text{-}11)$$

where P(w) is laser power, η_1 is an effective absorptivity representing the fraction of laser power transferred from the outer fibers to the resin, L_1(J/gm) is a heat of decomposition and sublimation, and κ is the thermal conductivity of the composite at right angles to the plies.

Equation (3-10) expresses our assumption that mass loss during low intensity radiations is mainly due to resin sublimation, and that this sublimation occurs at a constant rate per unit area. The left hand side of Equation (3-11) represents the rate at which energy is absorbed by the resin. The first term on the right represents power absorbed by the process of decomposition and sublimation. The second term on the right represents one-dimensional heat flow at right angles to the ply-planes (i.e. along the laser beam axis) and is evaluated by means of Equation (3-6). Thus, the results of our analysis of time-dependent temperature distributions are used directly in our description of low-intensity mass ablation.

We expect the effective absorptivity η_1 to be substantially less than unity, since heat conduction down the length of the outer fibers (i.e., transverse to the laser beam) must be appreciable. It is not evident that η_1 should be independent of the varying area $A'(t_e)$. Our assumption that it is a constant is based solely on our observation that two low intensity irradiations at the same power and exposure time but different beam spot radii produce the same mass loss.

Expressions for surface burn-area $A'(cm^2)$ and mass loss Δm(gm) follow directly from Equations (3-6), (3-10), and (3-11). Taking the partial derivative of $T-T_o$ in Equation (3-6) with respect to z and evaluating at $z = 0$ we obtain

$$A'(t_e) = \frac{\eta_1 P}{\gamma L_1} \left| 1 + \sqrt{\frac{4}{\pi}\, k\tau} \sum_{n=1}^{\infty} e^{-(n-\frac{1}{2})^2 k t_e} \right|^{-1} \qquad (3\text{-}12)$$

and

$$\Delta m(t_e) = \frac{\eta_1 P}{L_1} \int_o^{t_e} \left[1 + \sqrt{\frac{4}{\pi} k\tau} \sum_{n=1} e^{-(n-\frac{1}{2})^2 kt} \right]^{-1} dt, \qquad (3\text{-}13)$$

where, as in Section 3.3,

$$k = \pi^2 \kappa / \rho C_p \delta^2 , \qquad (3\text{-}8)$$

and where we introduce the definition

$$\tau \equiv \frac{1}{\pi} \rho C_p \kappa \left[\frac{T_m - T_o}{\gamma L_1} \right]^2 \qquad (3\text{-}14)$$

Equation (3-12) shows that the surface burn-area $A'(t_e)$ expands from a value of zero at exposure time $t_e = 0$ to an asymptotic limit at infinite exposure time, namely,

$$A'(t_e = \infty) = \frac{\eta_1 P}{\gamma L_1} . \qquad (3\text{-}15)$$

The constant τ (sec) is a characteristic time of the composite material and does not depend on the irradiation parameters or specimen thickness. From Equation (3-12) and a series approximation encountered in simple diffusion theory, it can be shown that τ^{-1} is a measure of the initial rate of growth of burn area relative to the asymptotic burn area at infinite exposure time; specifically,

$$\tau^{-1} = \left[\left(\frac{dA'}{d\sqrt{t_e}} \right)_{t_e=0} \Big/ A'(t_e=\infty) \right]^2 \qquad (3\text{-}16)$$

No simple expression has been found for the integral in Equation (3-13), which gives the mass loss Δm. However, we have developed an approximation which, based upon the size of the integrand as a function of kt_e, should yield an error of less than 2% of the actual value of the integral. The resulting approximation to Δm is

$$\Delta m(t_e) = \frac{\eta_1 P}{L_1} t_e \left\{ 1 - \frac{2\tau}{t_e}\left[\sqrt{\frac{t_e}{\tau}} - \ln\left(1 + \sqrt{\frac{t_e}{\tau}}\right)\right] \right\}, \quad kt_e \leq 2$$

$$= \frac{\eta_1 P}{L_1} t_e \left\{ 1 + \frac{4}{kt_e} \ln\left[\frac{\left(1 + \sqrt{\frac{4}{\pi}k\tau}\, e^{-\frac{1}{4}kt_e}\right)}{\left(1 + \sqrt{\frac{4}{\pi}k\tau}\, e^{-\frac{1}{2}}\right)}\right] \right. \qquad (3\text{-}17)$$

$$\left. - \frac{2\tau}{t_e}\left[\sqrt{\frac{2}{k\tau}} - \ln\left(1 + \sqrt{\frac{2}{k\tau}}\right)\right] \right\}, \qquad kt_e > 2$$

Our calculations of low-intensity burn areas and mass loss are based on Equations (3-12) and (3-17) respectively.

Numerical values of ρ, C_p, κ and $(T_M - T_o)$ for 5208/T300 already have been specified in Section 3.3 and the resulting values of the inverse time constant k have been listed for three different thicknesses. Then inspection of Equations (3-12), (3-14) and (3-17) shows that burn areas and mass losses can be calculated if we can obtain the parameters η_1, L_1 and γ. Our approach is to make an ab-initio estimate of the dissociation and sublimation energy L_1 based on the chemical structure of the resin and molecular bond-strengths cited in the literature. We then calculate η_1 and γ from mass losses observed in two of the low intensity irradiations.

We assume that 5208 resin consists of TGMDA with 32 gms of DDS curing agent per 100 gms of TGMDA. The molecular weight of TGMDA is 422.51 gms/mole. Each TGMDA molecule has 4 epoxy groups which we assume to open and form O-O bonds in curing. According to Pauling (Ref. 5) the strength of the O-O bond is 33.2 kcal/mole. Then liberating a TGMDA molecule

by thermal decomposition should require about 4(33,200) cal/mole TGMDA, or, since both TGMDA and DDS are evolved, a total energy per unit mass of about 4(33,200)/(1.32)(423) = 238 cal/gm. Since the extra energy required for sublimation of the decomposition products is negligible we therefore take

$$L_1 = 238 \text{ cal/gm} = 996 \text{ J/gm}$$

as the heat of decomposition and sublimation for 5208 resin.

In order to calculate values for η_1 and γ we use the above value of L_1 and average mass losses for 5 sec, 200 watt irradiations of 6- and 12-ply specimens obtained from Table 3-1, viz., 0.052 gm and 0.044 gm, respectively. Substituting these values, along with the above-specified values of ρ, C_p, and κ, into Equations (3-14) and (3-17), we obtain by simultaneous numerical solution

$$\eta_1 = 0.0778$$

and

$$\gamma = 0.0149 \text{ gm/cm}^2 \text{ sec}$$

It follows from Equation (3-14) that

$$\tau = 1.136 \text{ sec.}$$

The small value of the effective absorptivity η_1 is consistent with the expectation that heat flow along the length of the outer fibers (transverse to the beam) is large at low beam intensities, which correspond to relatively low fiber temperature and, consequently, relatively high fiber conductivity.

The measured and derived parameters which determine mass loss (Eq. 3-17) and surface burn area (Eq. 3-12) for low intensity exposures of 5208/T300 composite are summarized in Table 3-4. The parameters of this table also determine the on-axis time-dependent temperature distribution in accord with Equations (3-6) and (3-9).

Mass losses at low beam intensity have been calculated using Equation (3-12) and the parameters cited in Table 3-5. It is seen that the overall agreement is satisfactory. The last entry (from data of Ref. 14) is especially important, since it illustrates that our model applies reasonably well to high power (10000 watt) beams spread over an area large enough that the intensity falls into the "low" range. The comparisons at a beam power of 200 watts show that the model accounts for the experimentally observed increase in mass loss rate with increasing exposure time and decreasing specimen thickness. Both of these effects result from a "piling-up" of heat in the specimens.

Surface burn areas calculated by Equation (3-12) and the parameters of Table 3-4 are compared with values determined by the enhanced X-ray method in Table 3-6. It is seen that the agreement is reasonably good even though no burn area information was used in deriving the parameters of Table 3-4. Furthermore, the predictions appear to account fairly well for the experimentally observed decrease in burn area with increasing specimen thickness, laser power and exposure time being the same.

In summary, our model for low intensity laser interaction with composites successfully explains the following experimental results:

- On-axis back-surface temperature independent of beam spot size (intensity)
- Mass loss independent of beam spot size (intensity)
- Quantitative details of back surface temperature response as function of time
- Quantitative details of back surface temperature response as function of thickness

Table 3-4 Summary of Measured and Derived Parameters for Low Intensity Exposure of 5208/T300 Composite

T_o = initial specimen temperature = 20°C (typically)

T_M = temperature at which 5208 resin decomposes and sublimates = 350°C

ρ = composite density = 1.569 gm/cm^3

C_p = average specific heat between T_o and T_M = 1.214 J/gm°C

κ = average thermal conductivity across plies between T_o and T_M = 0.00383 watts/cm°C

η_1 = effective absorptivity (reduced by transverse heat flow) = 0.0778

γ = rate of resin mass sublimation per unit area = 0.0149 gm/cm^2 sec

L_1 = heat of decomposition and sublimation for resin = 996 J/gm

τ = burn area time constant = 1.136 sec

$k(sec^{-1})$ = inverse time constant characteristic of specimen thickness δ(cm) = $0.01985/\delta^2$

Table 3-5 Measured and Calculated Mass Loss at Low Beam Intensity: $I \leq I_L$ ($1100 < I_L < 1500$ w/cm^2)

Airflow (M)	Laminate	δ(cm)	P(w)	r(cm)	t_e(sec)	I(w/cm^2)	Δm(gm) (exp)	Δm(gm) (Eq.3-17)
0.2	$(0/\overline{+}45)_S$	0.094	200	0.25	5.0	1000	0.051	0.052
0.2	"	0.094	200	0.50	5.0	250	0.052	0.052
0.2	$(0/\overline{+}45)_{2S}$	0.185	200	0.25	10.0	1000	0.102	0.103
0.2	"	0.185	200	0.25	5.0	1000	0.045	0.044
0.2	"	0.185	200	0.5	5.0	250	0.043	0.044
0.2	$(0/\overline{+}45)_{4S}$	0.343	200	0.25	5.0	1000	0.041	0.044
0.2	"	0.343	200	0.50	5.0	250	0.033	0.044
0.3	$(0/\overline{+}45)_S$	0.094	10000	1.74	2.0	1050	0.73	0.81

All specimens painted; experimental Δm = average value;

δ(cm) = specimen thickness; P(w) = laser power; r(cm) = spot radius

I(w/cm^2) = beam intensity; t_e(sec) = exposure time; Δm(gm) = mass loss

Parameters used in calculation of Δm given in Table 3-4.

Table 3-6 Measured and Calculated Burn Areas
At Low Beam Intensity: $I \lesssim I_L$ ($1100 \; I_L \; 1500$ w/cm^2)

Airflow (M)	Laminate	δ(cm)	P(w)	r(cm)	t_e(sec)	I(w/cm^2)	A'(cm^2) (Exp)	A'(cm^2) (Eq. 3-12)
0.2	$(0/\overline{+45})_S$	0.094	200	0.25	5.0	1000	0.86	0.95
0.2		0.094	200	0.50	5.0	250	0.99	0.95
0.2	$(0/\overline{+45})_{2S}$	0.185	200	0.25	5.0	1000	0.78	0.72
0.2		0.185	200	0.50	5.0	250	0.75	0.72

All specimens painted; experimental surface burn area A' obtained by enhanced X-ray (TBE) measurement

δ(cm) = specimen thickness; P(w) = laser power; r(cm) = spot radius

I(w/cm^2) = beam intensity, t_e(sec) = exposure time; A'(cm^2) burn area

Parameters used in calculation of A' given in Table 3-4.

- Quantitative dependence of mass loss rate on exposure time
- Quantitative dependence of mass loss rate on specimen thickness
- Quantitative dependence of surface burn area on exposure time
- Quantitative dependence of surface burn area on specimen thickness

Finally, the model is qualitatively consistent with a "runaway" effect leading to its failure at high intensities because of fiber sublimation.

3.5 LASER INTERACTION AT INTERMEDIATE AND HIGH INTENSITIES

Our description of laser interaction with composites at low beam intensities fails at some intensity between 1100 and 1500 w/cm^2. As discussed in Section 3.2, we attribute this effect to the fact that the thermal conductivity of the exposed fibers decreases with increasing temperature. At sufficiently high intensities, heat flow along the length of the fibers (transverse to the beam) is quenched almost completely and the local fiber temperature rises rapidly to the point at which graphite sublimation is dominant.

In this section we develop a description of mass ablation and penetration rate which primarily is intended to apply to the highest intensities considered, namely, $I \geq 6000$ w/cm^2. In this range the burn hole is only slightly larger than the nominal burn radius, and radiative emissive power is small compared to the power absorbed in sublimation. Nevertheless, by taking radiative emission into account, while neglecting the difference between the burn hole radius and the beam spot radius, we expect to obtain a formalism which predicts mass ablation and penetration rate to the right order of magnitude even at intensities as low as 1500 w/cm^2.

Our general approach to composite ablation at high intermediate intensities is somewhat different than for the low intensity range. There, we developed a formalism and used a few experimental points to evaluate the unknown parameters. Here, we will obtain the parameters ab initio by using data on graphite sublimation taken from the literature on (non-laser) high temperature carbon effusion experiments. For the high intensity range we will treat mass ablation of aluminum in the same way. Because the absorptivity and emissivity of metals depends strongly on temperature, we have not established a satisfactory description of aluminum ablation in the low and intermediate intensity ranges.

For the intermediate and high intensity ranges we assume that (a) convective cooling is negligible, (b) thermal conduction is negligible, (c) the burn hole has the same radius as the beam spot, and (d) the heat of decomposition and sublimation of resin (in the case of composites) is small compared to that of graphite. Then, either for composite or aluminum, the rate of mass ablation per unit area satisfies the energy balance

$$I = \frac{1}{\eta}\left[(L_s + \Delta H) f \dot{\mu}(T) + \epsilon\sigma T^4\right] \qquad (3\text{-}18)$$

where

$I(w/cm^2)$ = beam intensity (Eq. 3-1)

$\dot{\mu}(gm/cm^2 sec)$ = rate of mass loss per unit area

$T(^oK)$ = absolute temperature of exposed surface

$L_S(J/gm)$ = sublimation heat of non-polymeric component

$\Delta H(J/gm)$ = heat to raise non-polymeric component to temperature T

f = mass fraction of non-polymeric component ($f = 0.7$ for composite, $f = 1$ for Al)

η = absorptivity for 10.6μ radiation at high temperature

ϵ = emissivity of exposed surface at high temperature

$\sigma = 5.669 \times 10^{-12}$ watt/cm^2 $^oK^4$ = Stefan-Boltzmann constant

We now assume that carbon or aluminum molecules are removed from the heated surface by convection and chemical reaction with air so rapidly that the sublimation is the same as it would be if the surface at temperature T(^{o}K) were in a vacuum. In this case, the rate of mass effusion per unit area, $\dot{\mu}(T)$, is related to the absolute vapor pressure of the hot surface in hypothetical equilibrium at temperature T(^{o}K) by the easily derivable expression

$$\dot{\mu} = \frac{\alpha}{f} \left(\frac{M}{2\pi RT}\right)^{\frac{1}{2}} p_e(T) \qquad (3\text{-}19)$$

where we have introduced the factor 1/f on the right to account for the fact that, in the case of composite, resin sublimates along with the fibers, thereby contributing to the mass loss. A factor f has been introduced into Equation (3-18) to cancel this factor, since we assume that the energy going into resin sublimation is negligible. The other symbols in Equation (3-19) are

α = an accommodation coefficient representing the probability that a molecule impinging on the surface will stick and be re-united to it

M(gm/mole) = molecular mass (or effective molecular mass) of the sublimating species

$R = 8.3143 \times 10^7$ erg/mole ^oK = universal gas constant

p_e(dyne/cm^2) = hypothetical absolute vapor pressure (or effective vapor pressure) over hot surface at temperature T(^{o}K) (due to sublimating species)

In general the hypothetical absolute vapor pressure has the form

$$p_e = p_\infty e^{-L'/R'T} \qquad (3\text{-}20)$$

where

p_∞ (dyne/cm^2) = hypothetical vapor pressure at infinite temperature

L'(cal/mole) = activation energy for sublimation

R' = 1.9865 cal/mole $^\circ$K = universal gas constant

Values of α, M, p_∞ and L' for graphite have been determined by experiments in which graphite specimens were heated electrically (Ref. 2, 3). A definitive paper by Thorn and Winslow (Ref. 3) gives effective values of α, L' and p_∞ calculated upon the assumption that the emitted molecules are monatomic carbon. The following set of parameters gives their measured effusion rates per unit area as a function of temperature regardless of the true composition of carbon vapor:

M = 12

α = 0.150

$p_\infty = 1.017 \times 10^{16}$ dyne/cm^2

L' = 182,500 cal/mole

Substitution of these values into Eqs. (3-19) and (3-20) provides a numerical expression for $\dot{\mu}$ as a function of temperature.

Thorn and Winslow also determined the composition of carbon vapor in the vicinity of 2400 °K. The vapor consists of C, C_2 and C_3 molecules with higher radicals being of minor importance. From the resulting empirical expressions for the partial pressures of these three components, the effective heat of sublimation of each component can be calculated, and the effective heat of sublimation per unit mass, L_s, can be estimated as a function of temperature. Specifically, the vapor pressures of each of the C_i components and their effective heat of sublimation H_i are given as follows (pressures expressed in atmospheres):

$$p_1(\text{atmos}) = 0.1390 \times 10^9 \; e^{-85719/T}; \; H_1 = 170.3 \text{ kcal/mole}$$

$$p_2(\text{atmos}) = 4.932 \times 10^9 \; e^{-97474/T}; \; H_2 = 193.6 \text{ kcal/mole}$$

$$p_3(\text{atmos}) = 6.471 \times 10^9 \; e^{-92785/T}; \; H_3 = 184.3 \text{ kcal/mole}$$

Defining the total pressure of all three species as

$$p = \sum_{i=1}^{3} p_i \tag{3-21}$$

and representing the molecular weight of C_i as $M_i(\text{gm/mole}) = 12i$, we can calculate the heat of sublimation per unit mass for graphite as a function of temperature by

$$L_S(\text{kcal/gm}) = \left[\sum_{i=1}^{3} H_i(p_i/p)\right] \Big/ \left[\sum_{i=1}^{3} M_i(p_i/p)\right] \tag{3-22}$$

From Equations (3-21) and (3-22), and the numerical expressions for p_i and H_i given above, we find that the heat of sublimation of graphite (on a mass basis) is virtually independent of temperature. For example the values of L_S, expressed in J/gm, at 2400°C, 3500°C and 3800°C are respectively 25,555 J/gm, 24,423 J/gm, and 24,358 J/gm. Thus we take

$$L_S = 24{,}400 \text{ J/gm}$$

for the heat of sublimation of graphite at all temperatures.

Equation 3-18 shows that we also need an estimate of ΔH, the heat required to raise the graphite fibers from their initial temperature to $T(^{\circ}K)$. Although this value, of course, depends on temperature, it is relatively small. From data on the specific heat of graphite at high temperature, we find that it varies from about 4500 J/gm at a final temperature of 2500°C to about 6600 J/gm at a final temperature of 3500°C. A reasonable average for the present application is

$$\Delta H = 5900 \text{ J/gm}$$

Thus, for graphite we take

$$L_S + \Delta H = L_2 = 30{,}300 \text{ J/gm}$$

where we have introduced the symbol L_2 to designate an effective heat of ablation.

For composite material the absorptivity η and the emissivity ϵ are approximately unity. A summary of all the above-specified parameters which determine the mass-ablation of composite through Equations (3-18), (3-19) and (3-20) is given in Table 3-7.

For the case of aluminum no value for the accommodation coefficient α has been found. Based on the high-temperature accommodation coefficients for other metals (Ref. 4) we assume that it is unity. By applying the Clapeyron-Clausius relation to aluminum vapor pressure data given in the Handbook of Chemistry and Physics we obtain

$$p_{\infty} = 5.183 \times 10^{11} \text{ dyne/cm}^2$$

$$L' = 71{,}200 \text{ cal/mole}$$

on the assumption that aluminum sublimates monatomically, i.e., M = 27 gm/mole.

Table 3-7 Parameters for Mass Ablation of Composite and Aluminum at Intermediate and High Beam Intensities

Parameter	Composite	Aluminum
η = absorptivity for 10.6μ radiation	1	1
ϵ = emissivity	1	1
f = mass fraction of non-polymeric component	0.70	1
α = accommodation coefficient of non-polymeric component	0.150	1
M(gm/mole) = effective molecular weight of non-polymeric component	12	27
p_{∞} (dyne/cm^2) = hypothetical vapor pressure of nonpolymeric component at infinite temp.	1.017×10^{16}	5.183×10^{11}
L'(cal/mole) = effective activation energy for sublimation of non-polymeric component	182,500	71,200
$L_S + \Delta H = L_2$(J/gm) = heat of ablation	30,300	11,625
ρ(gm/cm^3) = density	1.569	2.70
σ(w/cm^2°K^4) = Stefan Boltzmann constant	5.669×10^{-12}	
R(erg/mole°K) = universal gas constant	8.3143×10^7	
R'(cal/mole°K) = universal gas constant	1.9865	

Tabulations of the heat of sublimation, L_S, for aluminum show that L_S is approximately the same as the activation energy of sublimation, L', cited above. The heat required to bring aluminum to temperatures on the order of its sublimation temperature at normal pressure is roughly $\Delta H = 6$ kcal/mole. On this basis we obtain

$$L_S + \Delta H = L_2 = 11625 \text{ J/gm}$$

for the heat of ablation of aluminum. Since the sublimating metal is presumed to be in the molten state, it is reasonable to assume that the effective absorptivity and emissivity are roughly unity. Our high temperature ablation parameters for aluminum are summarized along with those for composite in Table 3-7.

Having estimated all of the high intensity ablation parameters for composites and aluminum, we now can obtain the mass ablation rates per unit area, $\dot{\mu}$, as a function of beam intensity I. If the radiative emission term in Equation (3-18) is negligible then $\dot{\mu}$ is simply proportional to I. But if the radiative emission term is not negligible, no simple relation expressing $\dot{\mu}$ in terms of I can be obtained. In principle, one would proceed by combining Equations (3-19) and (3-20), solving for T in terms of $\dot{\mu}$, then substituting this expression for $T(\dot{\mu})$ into Equation (3-18) and solving for $\dot{\mu}$ in terms of I. Since this approach is not feasible, we must relate $\dot{\mu}$ to I on a numerical basis. This is easily done by substituting arbitrary values of T into Equations (3-20), (3-19) and (3-18) and constructing a curve which expresses $\dot{\mu}$ in terms of I. This procedure yields, as by-products the surface temperature and radiative emission power as functions of beam intensity.

Calculations of $\dot{\mu}$ as a function of I for composite and aluminum, based on Equations (3-18), (3-19) and (3-20), and the parameters of Table 3-7, are shown in Table 3-8. We define the two parts of the power per unit area given by Equation (3-18) as

$$I_s = \frac{1}{\eta} (L_S + \Delta H) f \dot{\mu}(T) \qquad (3\text{-}23)$$

Table 3-8 Calculation of Mass Ablation and Radiative Emission at Intermediate and High Beam Intensities*

T(°C)	T(°K)	$\dot{\mu}$ gm/cm^{2}sec)	I_s(w/cm^2)	I_r(w/cm^2)	I(w/cm^2)
		Composites			
3100	3373	8.434 (-3	178.8	733.8	913
3200	3473	1.822 (-2	386.3	824.8	1211
3300	3573	3.764 (-2	798.0	923.9	1722
3400	3673	7.477 (-2	1585	1032	2617
3500	3773	1.431 (-1	3034	1149	4183
3600	3873	2.648 (-1	5614	1276	6890
3700	3973	4.752 (-1	10074	1412	11486
3800	4073	8.280 (-1	17554	1560	19114
3900	4173	1.404 (0	29765	1719	31484
4000	4273	2.323 (0	49248	1890	51138
		Aluminum			
1900	2173	1.737 (-1	2019	126	2145
2000	2273	3.509 (-1	4079	151	4230
2100	2373	6.675 (-1	7766	180	7940
2200	2473	1.204 (0	13997	212	14209
2300	2573	2.073 (0	24099	248	24347
2400	2673	3.426 (0	39827	289	40116
2500	2773	5.454 (0	63403	335	63738
2600	2873	8.403 (0	97685	386	98071

*From Equations (3-18) - (3-25) and the parameters of Table 3-7, burn hole radius assumed equal to beam spot radius. T = temperature in burn hole; $\dot{\mu}$ = mass ablation rate per unit area; I_s = power per unit area absorbed by sublimation; I_r = radiative emission per unit area; $I = I_s + I_r$ = beam intensity. Radiative power = $\pi r^2 I_r$, with r = beam spot radius.

and

$$I_r = \frac{1}{\eta} \epsilon \sigma T^4 \tag{3-24}$$

These expressions represent the part of the beam intensity I which is translated into sublimation and radiative emission respectively. Thus, the radiative power emitted from the beam spot is given by

$$P_r = \pi r^2 I_r \tag{3-25}$$

where r(cm) is the beam spot radius.

For the case of composites Table 3-8 shows that, even though the radiative emission increases as T^4, it becomes small relative to sublimation power at high beam intensities. In the case of aluminum the radiative emission power is relatively small at all beam intensities to which the model applies.

The calculated mass ablation rates per unit area are shown as a function of beam intensity in Figure 3-5. Also shown in Figure 3-5 are the mass ablation rates deduced from experimental mass losses and burnthrough times shown in Tables 3-1, 3-2, and 3-3 on the assumption that the burn hole radius is the same as the beam spot radius, r. Specifically, for non-burnthrough shots the experimental points in Figure (3-5) are represented by

$$I = P/\pi r^2, \quad \dot{\mu} = \Delta m/\pi r^2 t_e \tag{3-26}$$

where t_e is the exposure time. For burnthrough shots the experimental points are represented by

$$I = P/\pi r^2, \quad \dot{\mu} = \rho \delta / t_b \tag{3-27}$$

where ρ is specimen density, δ is specimen thickness and t_b is time to complete burnthrough.

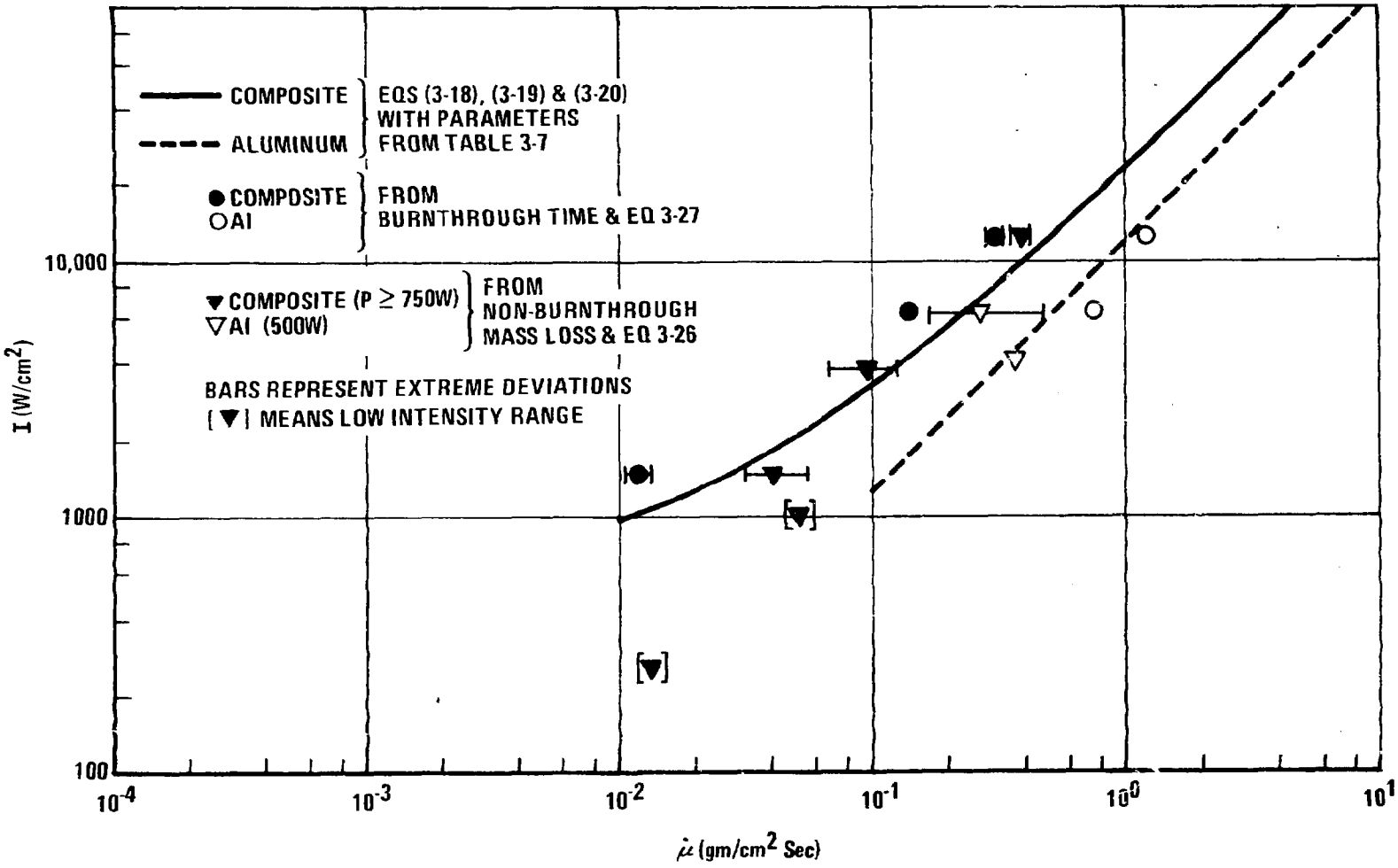

Figure 3-5 Calculated and Measured Mass Ablation Rates at Intermediate and High Intensity

Figure 3-5 includes two points taken from the low intensity mass loss data for composites given in Table 3-1. It is seen that the representations of the experimental values at low intensity are well below the predicted curve. It is probably accidental that a downward extrapolation of the linear part of the $\dot{\mu}(I)$ curve for composites (corresponding to absence of thermal emission) would pass near these points. However this happenstance may be used to advantage in defining a dimensionless parameter for mechanical characterization, since for the sake of simple correlation it is desirable to characterize burn dimensions on the basis of the ablation heat $L_2 = L_S + \Delta H$ without introducing the complicating effect of radiative emission.

For high and intermediate intensities the overall agreement between experiment and our ab-initio predictions is satisfactory. The fact that the values of $\dot{\mu}(I)$ deduced from burnthrough and non-burnthrough shots at an intensity of about 1500 w/cm^2 (intermediate range) do not agree with each other is partly due to our assumption that the burn hole radius is equal to the beam spot radius. At high intensities the prediction is rather good both for composite and aluminum. It is seen that the agreement for composites could be made even better by assuming the absorptivity η to be 0.75 instead of unity.

3.6 SUMMARY OF THERMAL CHARACTERIZATION

We have shown that correlation of our experimental data on temperature response, mass loss, and penetration time requires a division of the laser beam intensity (power density) I into three ranges. These are

Low Intensity Range: $I < I_L$ $(1100 < I_L < 1500$ w/cm$^2)$

Intermediate Intensity Range: $I_L \leq I \leq I_H$ $(1500 < I_H < 6400$ w/cm$^2)$

High Intensity Range: $I_H < I$ $(1500 < I_H < 6400$ w/cm$^2)$.

In the low intensity range our model applies only to composites. Mass loss for exposure times on the order of seconds is primarily due to resin ablation. Parameters applicable to this range are given in Table 3-4. Temperature response along the beam axis is satisfactorily predicted as a function of exposure time and specimen thickness by Equations (3-6) and (3-9). Mass loss and surface burn areas are predicted satisfactorily as a function of exposure time and thickness by Equations (3-17) and (3-12) respectively.

Our explanation for the transition from the low to the intermediate range behavior involves a "runaway" effect resulting from the fact that the thermal conductivity of exposed graphite fibers along their length (transverse to the beam) decreases with increasing temperature. Thus, composite exposures in the intermediate range are characterized by a period in which only resin is sublimated, followed by a period in which fibers are sublimated. Prolonged exposures of composites in the intermediate range therefore produce effective burn hole radii which are appreciably larger than those of the beam spots. We obtain order of magnitude agreement for mass ablation and penetration in the intermediate range by treating them the same as in the high intensity range (see below). In the intermediate range a significant part of the laser beam energy goes into radiative emission.

Our model for mass ablation and penetration in the high intensity range applies both to composites and aluminum. Its conceptual validity is supported by the fact the mass ablation parameters were obtained ab initio from non-laser-induced sublimation data. In this range the laser interaction resembles a drilling-process, the effective burn hole radius being only slightly larger than the beam spot radius. Power going into radiative emission is small compared to power going into sublimation. Therefore mass ablation and penetration are characterized by an effective heat of ablation. Taking radiative emission into account, we find that the aluminum data at high intensities and the composite data at both high and intermediate intensities are predicted reasonably well by Equations (3-18), (3-19) and (3-20) with the parameters given in Table 3-7. By-products of calculations include the burn hole temperature and radiative emission power.

In regard to the composite data at low beam intensities it should be noted that some sublimation from the outer fibers was evident, even though the model which successfully predicts temperature response and mass ablation rates assumes that only resin is sublimated. However, we estimate that the mass of fiber removed in all cases was less than 25% of the resin mass loss. Although our low intensity irradiations during this program involved only beam spot sizes of 0.25 and 0.5 cm, a high power, low intensity data point from Reference 14 shows that our low intensity model applies to much larger spot sizes.

For all three intensity ranges our model assumes that convective cooling is not important. In the case of composites, this assumption is supported by a few experimental data taken at different airflow velocities. In the case of aluminum the effects of airflow may be significant because of the strong dependence of beam absorptivity on the oxidation state of the sublimating surface.

4. MECHANICAL CHARACTERIZATION

In this section we present all results of the mechanical testing of laser-damaged coupons. After an opening discussion of the control experiments on undamaged and notched coupons, and an examination of various techniques to describe notched laminate behavior, we explore various parameters with which to correlate our observed laser-induced strength reduction. The strengths are shown to be described by a dimensionless parameter which depends on incident beam intensity, beam spot size, and specimen thickness. This parameter may be directly interpreted in terms of a hole radius and hole depth. The laser-damaged results are thus predictable in the sense that they may be compared to the drilled controls. We then compare composite and aluminum strength retention, examine the effects of preload, and comment on the relationship of the present results to previous work.

4.1 CONTROL EXPERIMENTS

Baseline static tensile data were obtained at room temperature on the 1 inch by 9 inch graphite-epoxy coupons loaded through bonded fiberglass tabs at each end. Both unnotched specimens and specimens containing drilled holes were tested. Three replicates were tested at each condition using a load rate of 0.05 inch/minute.

Three thicknesses of $(0/\pm45)_C$ unnotched control specimens were tested providing the following average failing stresses.

$(0/\pm45)_S$	70.0 ± 2.0 KSI
$(0/\pm45)_{2S}$	76.9 ± 1.3 KSI
$(0/\pm45)_{4S}$	75.0 ± 7.2 KSI

These data were combined to form an average unnotched tensile strength of 74.0 KSI. Notched tests were also conducted on $(0/\pm45)_S$ and $(0/\pm45)_{4S}$ laminates containing 0.125 inch and

0.250 inch diameter holes drilled completely through the coupon centered at midlength. The following average failing stresses were obtained:

$(0/\pm45)_S$	0.125 inch dia.	48.2 ± 4.4 KSI
	0.250 inch dia.	36.2 ± 1.2 KSI
$(0/\pm45)_{4S}$	0.125 inch dia.	46.2 ± 0.6 KSI
	0.250 inch dia.	37.5 ± 0.8 KSI .

The same series of tests were also conducted on a $(90/\pm45)_{2S}$ laminate with the following results:

$(90/\pm45)_{2S}$	Unnotched	36.9 ± 0.4 KSI
	0.125 inch dia.	27.2 ± 0.5 KSI
	0.250 inch dia.	20.1 ± 0.3 KSI

These data are plotted in Figure 4-1 and are compared with three data reduction techniques commonly used for analyzing the notched behavior of advanced composite laminates. The method outlined in Reference 4 employs the existing fracture mechanics stress intensity solution for a circular hole with edge cracks to model the notched behavior. Two data points are used to determine the unknown parameters in the solution which then predicts the behavior of the remaining data. In this instance the unnotched data and the 0.250 inch diameter hole data were used to define the unnotched strength and the material parameter, a.

The material parameter, a, is defined by the following equation (Reference 9),

$$\frac{\lambda\sigma_N}{\sigma_o} = 0.295 + \frac{0.705\left(\frac{a}{R}\right)}{\left[1 + \left(\frac{a}{R}\right)^{1.2}\right]^{.8333}} \qquad (4\text{-}1)$$

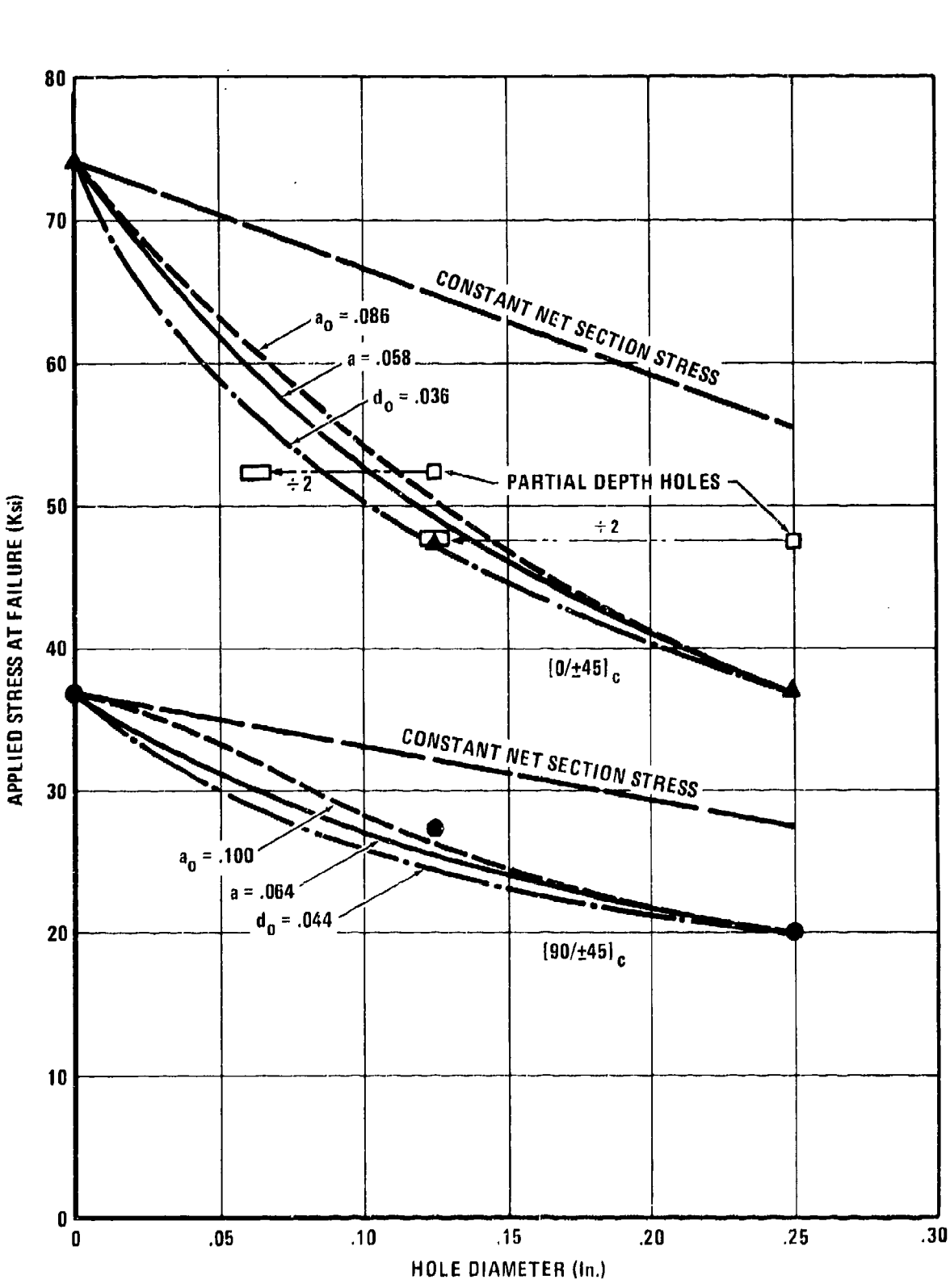

Figure 4-1 Behavior of Control Laminates

where

λ = Factor correcting finite width result to infinite plate result,

σ_N = Notched laminate failing stress of finite width coupons,

σ_o = Unnotched laminate failing stress,

a = Material parameter,

and R = Hole radius.

The width correction factors, λ , obtained from Reference 10 are tabulated below.

TABLE 4-1

Width Correction Factors for Notched Laminates

	HOLE DIAMETER (in.)	
Laminate	0.125	0.250
$(0/\pm45)_c$	1.05	1.11
$(90/\pm45)_c$	1.06	1.07

Iterating Equation (4-1) to determine the material parameter, a, yields values of a = 0.058 in. and 0.064 in. for the $(0/\pm45)_c$ and $(90/\pm45)_c$ laminates, respectively.

The predicted behavior as indicated by the solid curve in Figure 4-1, is 4.0 percent high for the $(0/\pm45)_c$ laminate and 6.7 percent low for the $(90/\pm45)_c$ laminate, considering the 0.125 inch diameter hole.

A second method for analyzing notched data discussed in Reference 11 is called the "point stress criterion." Again two data points are used to define the unnotched strength and a material parameter, a_o, which represents the distance from the edge of the hole to the point on the stress distribution across the net section whose magnitude equals the unnotched strength. The parameter, a_o, is defined by the following equation (Reference 11),

$$\frac{\lambda\sigma_N}{\sigma_o} = \frac{2(1 - \xi_2)}{2 - \xi_2^2 - \xi_2^4 + (K_T^\infty - 3)(\xi_2^6 - \xi_2^8)} \qquad (4\text{-}2)$$

where

$$\xi_2 = \frac{R}{R + a_o} ,$$

and K_T^∞ = Infinite plate stress concentration factor associated with net-section failure.

All other terms are defined as before.

Iterating Equation (4-2) to determine a_o provides values of 0.086 in. for the $(0/\pm45)_c$ laminate and 0.100 in. for the $(90/\pm45)_c$ laminate. The predictions made with this method are 7.0 percent high for the $(0/\pm45)_c$ laminate and 3.8 percent low for the $(90/\pm45)_c$ laminate, both containing a 0.125 inch diameter hole.

A third method (Reference 11) known as the "average stress criterion" is similar to the second method except that the parameter, d_o, is the distance from the edge of the hole to a point on the stress distribution across the net section such that the average stress over that distance equals the unnotched strength.

The parameter, d_o, is defined by the following equation (Reference 11),

$$\frac{\lambda\sigma_N}{\sigma_o} = \frac{2}{2 + \xi_1^2 + 3\xi_1^4 - (K_T^\infty - 3)(5\xi_1^6 - 7\xi_1^8)}, \qquad (4\text{-}3)$$

where

$$\xi_1 = \frac{R}{R + d_o}.$$

All other terms are defined as before.

Iterating Equation (4-3) to determine d_o gives values of 0.036 in. for the $(0/\pm45)_c$ laminate and 0.044 in. for the $(90/\pm45)_c$ laminate.

These predictions for the 0.125 inch diameter hole are 11.0 percent low for the $(90/\pm45)_c$ laminate and extremely close for the $(0/\pm45)_c$ laminate.

Interestingly enough, the average error for all three methods is very nearly the same, $\pm$ 5.4 percent. The straight line in Figure 4-1 represents a constant net section stress failure criterion which works well for ductile materials such as aluminum, but obviously is inappropriate for advanced composite laminates whose stress-strain behavior is essentially linear to failure.

Two additional specimen configurations were tested with the $(0/\pm45)_c$ laminate. Holes measuring 0.125 inch and 0.250 inch in diameter were drilled through only one-half of the specimen thickness. These test results are plotted as open squares in Figure 4-1. One possible way of predicting these strengths is to assume an effective hole diameter which is less than the actual diameter of the drilled hole and is a function of hole depth. For example, if an effective hole diameter were chosen to be one-half the actual hole diameter, (these holes are through only one-half the specimen thickness) the measured values would be within approximately 3 and 12

percent of the solid curve prediction as indicated by the "÷2" rectangles in Figure 4-1. As we will see in later paragraphs of this section, this approach for characterizing partial depth holes, i.e., reducing the hole diameter by a factor which accounts for its depth, may be tenable.

In summary for the composite controls, the unnotched and drilled hole static tension data appear to be consistent with the expected behavior of the 5208/T300 material system for both the $(0/\pm45)_c$ and $(90/\pm45)_c$ laminate configurations. All three data reduction methods are appropriate for modeling the behavior of these laminates containing through the thickness drilled holes and likely can be modified to account for the effects of partial depth holes. Since the prediction given by the solid curve in Figure 4-1 falls roughly midway between the other two, and since all three predictions are similar, we will hereafter use the prediction of Reference 4 which employs the existing fracture mechanics stress intensity solution for a circular hole with edge cracks.

Notched and unnotched 2024(T81) aluminum coupons (three specimens/condition) were similarly employed to obtain control data for comparison with the composite results. Table 4-2 summarizes the unnotched and drilled aluminum results.

Table 4-2 Results for Aluminum Tensile Specimens (Controls)

Specimen	Gross Failure Stress (KSI)	$\frac{\sigma_N}{\sigma_o}$	Fractional Net Section (Measured)
Unnotched	73.2	1.0	
0.250 in. dia. drilled through	55.3	.76	.75
0.125 in. dia. drilled through	64.8	.88	.87
0.250 in. dia. half through	64.8	.88	.88
0.125 in. dia. half through	69.0	.94	.94

The comparison of strength retention (σ_N/σ_o) with the fractional cross section of the specimen remaining after drilling confirms the anticipated behavior for this ductile material, i.e., constant net section failing stress equal to unnotched strength.

4.2 LASER-DRILLED THROUGH HOLES - SOME BACKGROUND

The case in which composite specimens are completely penetrated by the laser beam is worth brief discussion, for it provides an interesting base from which to proceed to situations where only partial penetration occurs.

An interesting simulation of through penetration is provided by Whitney and Kim (Ref. 12), who showed that temperatures from 75°F to 550°F had little effect on the strength of $(0/\pm45/90)_S$ laminates of Hercules AS/3501-5 containing through drilled holes. Based on these data, they concluded that through-penetration by a high energy heat source (such as a laser) could be characterized for purposes of strength retention as a conventional drilled-hole of the same size. They also noted that notch sensitivity is reduced with increasing temperature and suggested that as the temperature increases, the matrix becomes increasingly degraded. This makes loading of the 0° fibers above and below the hole more difficult and in fact their data suggest a transition toward constant net section failing stress as the temperature increases. One further point of their work worth noting is that preloads at the high temperatures they used have little effect on the room temperature strength. We will see that this result agrees well with our data for strength retention of specimens irradiated, but not fractured, under load.

Another background reference worth noting at this point is the previously-mentioned work of Ender, et al (Ref. 3) of MCAIR, who investigated various aspects of laser damage in 5208/T300 $(0/\pm45/90)_S$ laminates. In many cases there, the beam intensities and spot sizes overlapped the present work, although their strength retention measurements concentrated on specimens completely penetrated.

Two conclusions of the MCAIR report are quite pertinent. The first relates to strength retention compared to (2r/w) and (l/w), where r is the through hole radius, w the specimen width, and l the diameter of the heat affected zone. They found that predicted strength retention agrees with experiment when the actual hole size (2r) is used, but not when the apparent damage size (l) is used. This result is somewhat comparable to the Whitney-Kim work, and emphasizes that the strength of a drilled composite is predictable in the same way for conventional holes as for high-intensity laser-drilled holes. We stress, however, that the lowest power density used by Ender for these results was 1.8 kw/cm^2.

The second conclusion to note from Reference 3 is that burnthrough with small ($\sim$ 1 cm^2) beams requires two to three times the energy density as burnthrough with large (6-10 cm^2) beams for power densities below 6 kw/cm^2. They suggest that considerable energy is lost from the smaller regions by radial conduction. Their data show that the beam intensities required for burnthrough with different beam areas tend to converge at intervals around 6 kw/cm^2. This suggests that our intensity I_H which designates the upper limit of the "intermediate energy range" defined in Section 3 and which is assigned the upper bound of 6.4 kw/cm^2 actually has a value on the order of 6 kw/cm^2. The present work thus provides interesting comparison with that of Reference 3.

4.3 PARTIAL-PENETRATION LASER DAMAGE IN COMPOSITES

In 4.2 we briefly discussed the typical situations in which one examines the effects of laser-induced damage consisting of full depth holes. That damage is conveniently characterized by the radius of the hole. For constant energy exposures, the strength reduction might be relatable simply to energy density (e.g. kj/cm^2), since this parameter will describe the hole size in that case. For scenarios which involve a considerable range of laser power, exposure time, spot size, and specimen characteristics (such as thickness and layup), it is clear that severable variables must enter.

We thus must address the following question: how may strength retention of laser-damaged advanced composite materials be described in the general case where the material is not completely penetrated?

4.3.1 Parameterization of Partially-Through Holes

Many structural applications of advanced composites rely on a directional strength property of the material. A common laminate for such purpose would be the $(0/\pm 45)_c$ employed here as our baseline specimen. Since this laminate is fiber-dominated, i.e., its longitudinal strength is primarily determined by the 0^o fibers, it is worthwhile to consider the effect of removing certain percentages of 0^o fibers from the cross section. If in fact the laminate tensile strength were solely governed by the 0^o fibers, we might expect a net section strength reduction as successive fractions of those fibers were removed.

In Figure 4-2, we plot the strength retention σ_R/σ_o (ratio of residual tensile strength to undamaged tensile strength) as a function of the percentage of 0^o fibers removed from the cross-section. This percentage was determined on selected specimens by measuring the transverse dimensions of ablated 0^o fibers throughout the depth of the burn. Also plotted in the figure are the drilled-hole results from the control experiments. The curves are arbitrary and show the trends only. We have made no distinctions here between different spot sizes or exposure times.

It is interesting to observe that the high-power data seem to follow a straight line as we would expect for a constant net section failing stress, but note that the slope of that line is twice as great as one would expect on that basis. The 750 watt data fall far below that line and would suggest a strength retention dependent on stress concentration. The primary difference between those data sets is the generally-longer exposure times at the lower power to achieve equivalent fiber removal. Note that no 200 watt data appear since there was essentially no fiber removal in that case.

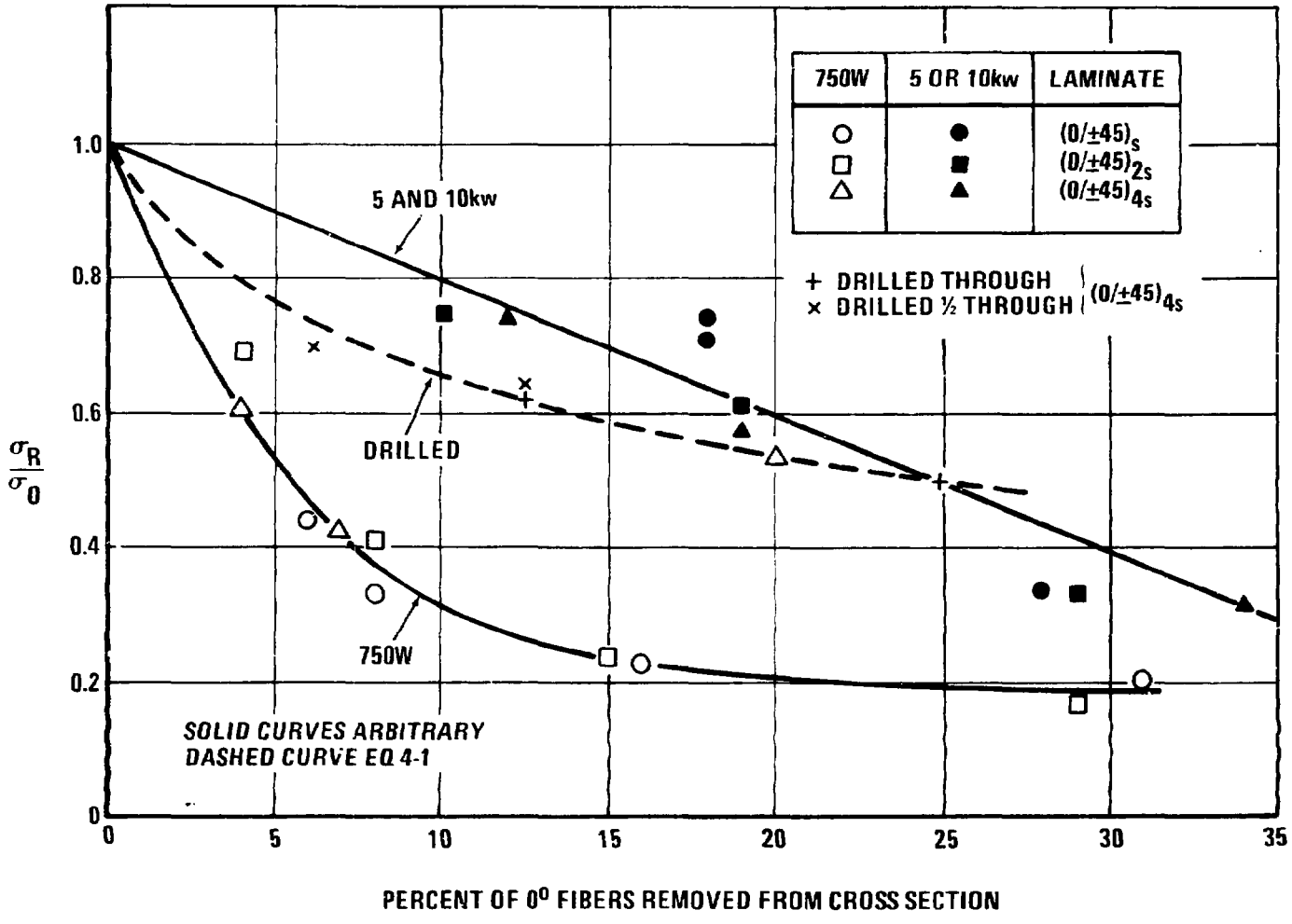

Figure 4-2 Dependence of Strength Retention for $(0/\pm45)_c$ on Removed 0° Fibers

Two conclusions are clear from this figure, namely that (1) even for fiber-dominated laminates, laser-induced fiber removal is not a generally-applicable parameter for characterization, and (2) the contribution of the epoxy matrix to the strength is considerable.

The last point bears brief comment. McKague (Ref. 13) has shown that for tows (3000 fibers) of Thornel 300, gauge length 9 inches, loaded in tension, the dry tows failed at an equivalent fiber stress of 61 ksi, while epoxy-impregnated tows failed at an equivalent fiber stress of 360 ksi. The matrix thus serves to distribute shear load between fibers and dramatically contributes to the tensile strength.

It is clear that fiber removal in laser damage is only part of the description, for both removed matrix and adjacent heat-affected matrix must also contribute. The limiting case of this effect occurs in some of our 200 watt exposures. As we will see there, even though only the matrix is damaged (i.e., no fiber ablation), the strength reduction is marked. We must therefore proceed to damage characterizations which consider the material as a whole, rather than one which relies only on fiber characteristics.

From other through-hole results and from our drilled (through and partial) controls, it is reasonably clear that one needs a damage characterization parameter which depends on some "hole" size r, and a hole depth h. To relate specimens of different thickness, it is clear that a total thickness δ must appear also. If the partial depth description is to yield the through-hole result as $h \to \delta$, then it is reasonable to consider the simplest possible parameter, namely rh/δ. We thus suggest that the tensile strength retention for laser-damaged composites be describable as a function of this parameter. In the limiting case where $h = \delta$ (through hole), the strength retention is then given by Eq. 4-1, which depends only on the hole radius and the "constant" material parameter a determined from notched control experiments.

From Equations 3-26 and 3-27 of Section 3 we can write

$$\Delta m = \pi r^2 \left(\frac{t_e}{t_b} \right) \rho \delta \ . \qquad (4\text{-}4)$$

If we assume that the effective depth of penetration, h, is proportional to the exposure time, t_e, then

$$\Delta m = \pi r^2 \rho \left(\frac{h}{\delta}\right) \delta \ , \text{ or}$$

$$\frac{\Delta m}{\pi r^2} = \rho \left(\frac{h}{\delta}\right) \delta \ . \qquad (4\text{-}5)$$

For a suitable range of intensities, we have also shown that the mass loss Δm is proportional to the total incident energy E, so we expect that

$$\frac{E}{\pi r^2} \propto \left(\frac{h}{\delta}\right) \delta \rho . \qquad (4\text{-}6)$$

This shows, as expected, that the penetration depth h is proportional to the energy density. If we expect the damage parameter to depend on radius, then we must multiply both sides by r, and the relation 4-6 becomes:

$$\left(\frac{E}{\pi r^2}\right)\left(\frac{1}{\rho \delta}\right) r \propto \frac{rh}{\delta} \ . \qquad (4\text{-}7)$$

The parameter on the left of Eq. 4-7 contains the expected variables of energy density, radius, and specimen thickness.

A comment is due at this point on the significance of the radius, r, which appears. We have tacitly assumed that r is some kind of hole radius, but is it the radius of the beam spot, or some effective damage radius? This consideration is further complicated by the fact that two "types" of beams were employed for these investigations. The intensity profile at 200 and 750 watts was essentially Gaussian, while that at 5 and 10 kw was square. For describing results with these two beam types on the same basis, we will define an effective radius

$$r_e = \begin{cases} r \text{ for the 5 and 10 kw beam} \\ \frac{2}{3} r \text{ for the 200 and 750 beams,} \end{cases} \qquad (4\text{-}8)$$

where r is the nominal beam radius measured from plexiglass burns. The latter number 2r/3 is based on examination of the lower power burns in plexiglass and estimating the effective radius if all the Gaussian intensity were concentrated in an equivalent square profile.

In order to distinguish these beam radii from an actual damage radius as measured by radiopaque enhanced X-rays of the damaged specimens, we will use R for that radius.

4.3.2 Strength Retention of Laser-Damaged Composites - $(0/\pm 45)_c$

In this subsection we will investigate the following parameters (Table 4-3) to describe strength retention of our graphite-epoxy composite tensile specimens after laser damage. Each of these parameters is relatable to a "hole" radius times depth, normalized to specimen thickness, and may thus be compared with our drilled hole results.

Table 4-3 Damage Characterization Parameters

Parameter	Units	Description
$\frac{\Lambda m}{\pi \rho \delta R}$	cm	R is the transverse radius of the damage area as measured by TBE/X-ray. This parameter depends only on specimen measurements.
$(\frac{E}{\pi r_e^2})(\frac{r_e}{\delta})$	kj/cm^2	E is the total incident laser energy and r_e is the effective beam radius given by Eq. 4-8; this parameter depends only on beam characteristics, except for known specimen thickness δ.
$\frac{\Lambda m}{\pi \rho \delta r_e}$	cm	This parameter depends on both specimen measurements and laser beam spot size.

In Figure 4-3, we compare the strength retention for the $(0/\pm45)_c$ composites with our drilled hole prediction (Eq. 4-1) using the first parameter listed in Table 4-3. We note in this case that this characterization indicates greater strength reduction for a given R than we might expect. The drilled hole prediction in this case gives somewhat of an upper bound to the strengths, whereas a lower bound would be more useful from a design standpoint.

In Figure 4-4, we plot strength retention as a function of incident laser beam characteristics. The curves shown are arbitrary. The parameter used there cannot be directly related on this plot to hole size, because of its units. If it were divided by an effective heat of ablation and material density, a direct comparison may be made. We explore this in the following subsection. The curves drawn do serve to indicate the different results for the 200 watt/0.8 cm^2 burns compared to all other data. There seems no doubt that "low" intensity "large" beams are unusually effective in causing strength reduction.

Figure 4-5 shows the strength retention as a function of the final parameter from Table 4-3. In this case the drilled hole prediction describes the data rather well, and in fact tends to the low side in strength prediction. The parameter itself is not a particularly useful one, however, since it requires knowledge of the beam spot size and measurement of the specimen mass loss.

We have deleted from these plots those data which represent "unusual" irradiation conditions, such as significantly different air flow, irradiation of unpainted side, and high moisture content specimens. The results for these sets of exposures are listed in Table 4-4. For each set of laminates shown, all experimental conditions were the same, except as listed.

These limited results indicate that there is little difference in residual strength if the damaged surface is unpainted or if the laminate has an unusually-high moisture content. In the last set, e.g., one group of three laminates was immersed in water for four months prior to exposure. The moisture content rose to 0.7% by weight, which is roughly

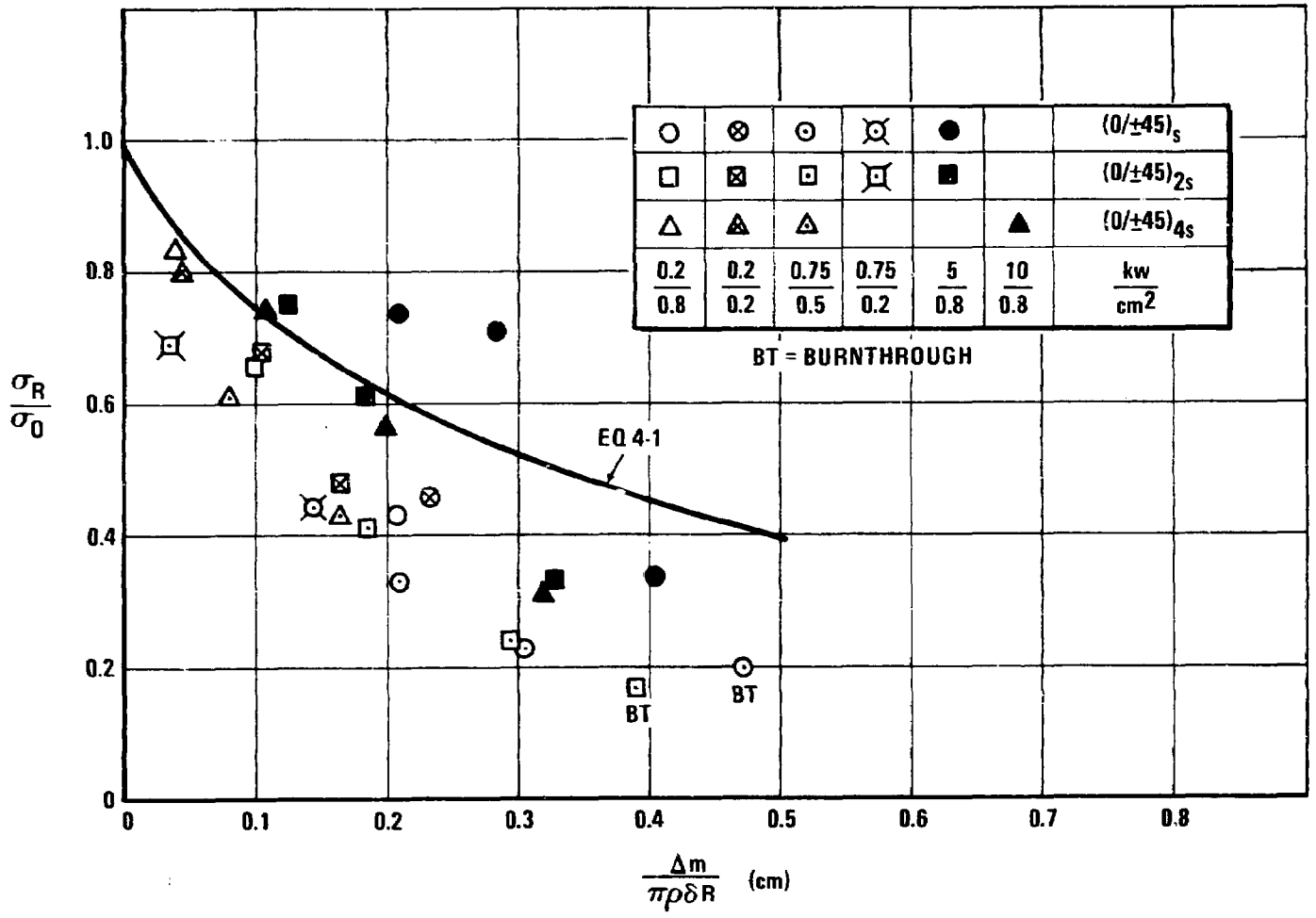

Figure 4-3 Strength Retention for $(0/\pm45)_c$ vs Measured Damage Size

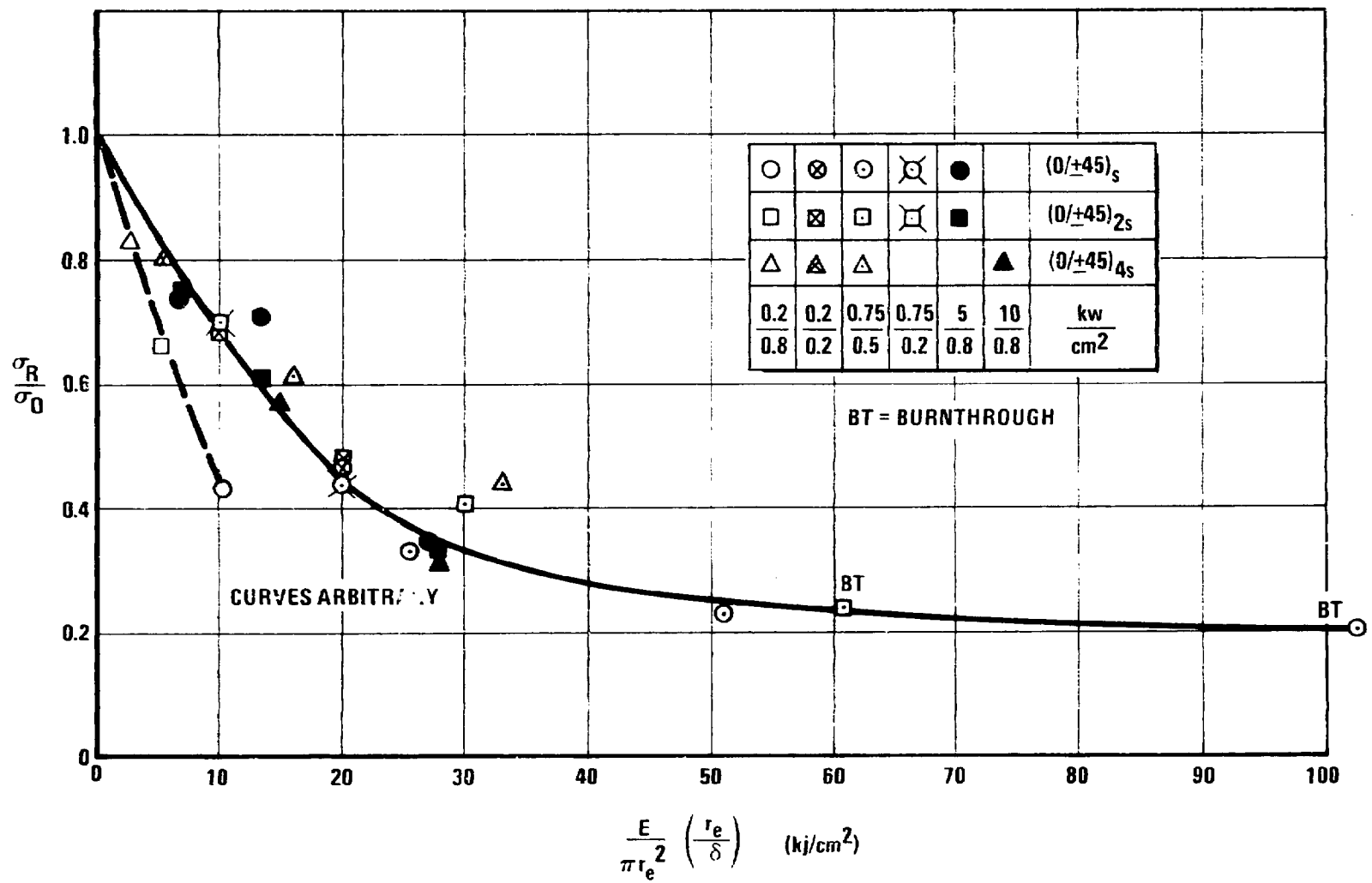

Figure 4-4 Strength Retention for $(0/\pm45)_c$ vs "Normalized" Energy Density

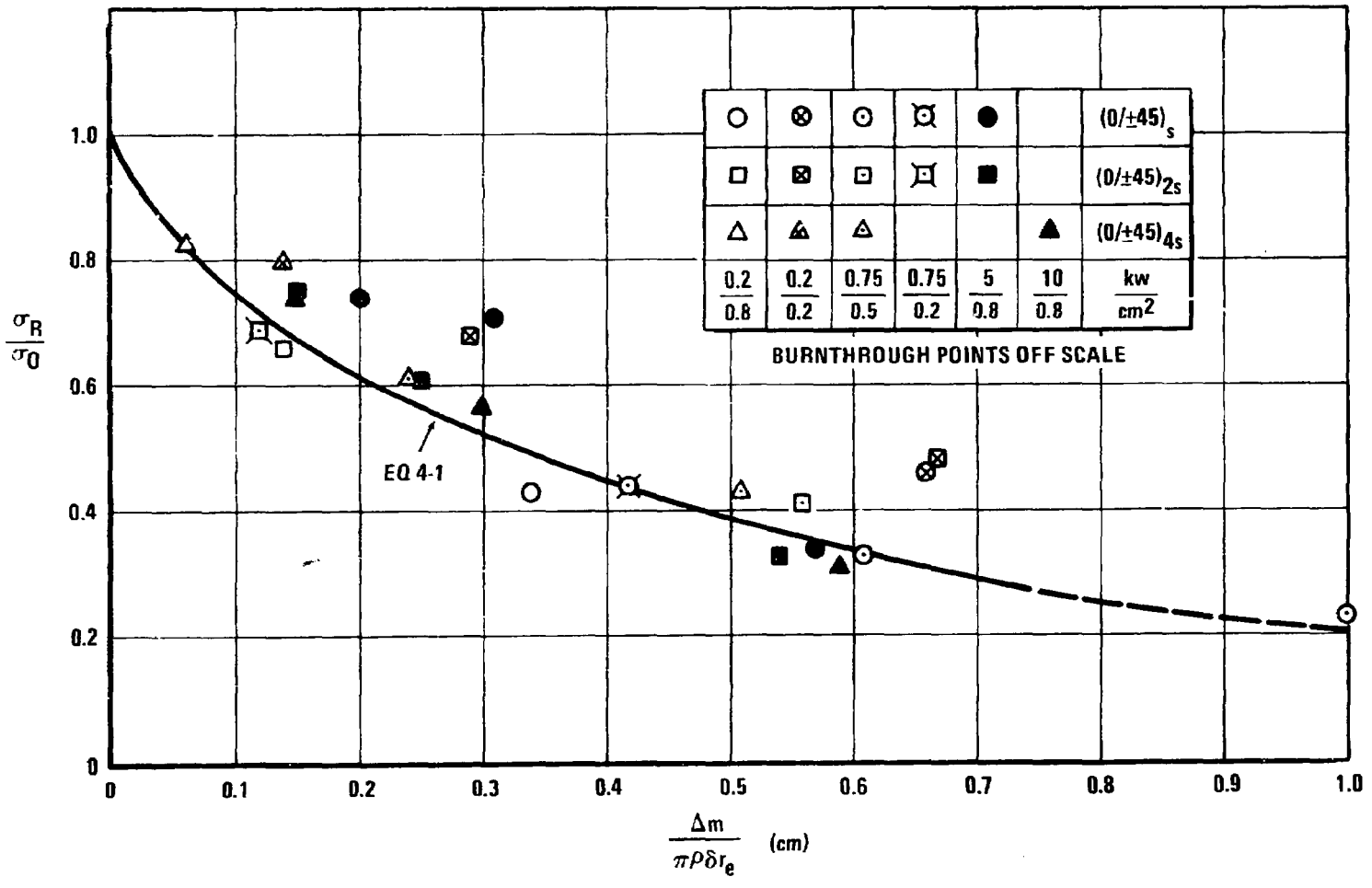

Figure 4-5 Strength Retention for $(0/\pm45)_c$ vs Mass Loss/Beam Size Parameter

Table 4-4 "Unusual" Exposures

Laminate/Condition		Power (kw)	Time (sec)	σ_R/σ_o
$(0/\pm45)_{4S}$	Painted Side	.750	12.8	.43
	Unpainted Side			.47
$(0/\pm45)_{4S}$	Airflow -0.3M	10	0.8	.57
	Airflow -0.9M			.54
$(0/\pm45)_{2S}$	"Dry"	5	0.8	.61
	0.7% Moisture			.60

equivalent to what one might expect for one-sided exposure for approximately 6 months at a location such as Guam. These data in Table 4-4 also suggest there is little effect of high airflow during such laser exposures. This point will be discussed further in paragraph 4.4.

4.3.3 Strength Retention for Laser-Damaged Composites - $(90/\pm45)_c$

Thus far we have primarily addressed laser damage in the fiber-dominated $(0/\pm45)_c$. We here will briefly discuss the results for the matrix-dominated $(90/\pm45)_c$.

In Figure 4-6 we plot the strength retentions for laser-damaged $(\pm45/90)_{2S}$ and $(90/\pm45)_{2S}$ laminates. The data scatter is considerable, but this is not unexpected for matrix-dominated composites. Our experience in other programs indicates that the coefficient of variation in strengths for "identical" specimens is about twice as great for this type of coupon as far ones which fiber-dominated.

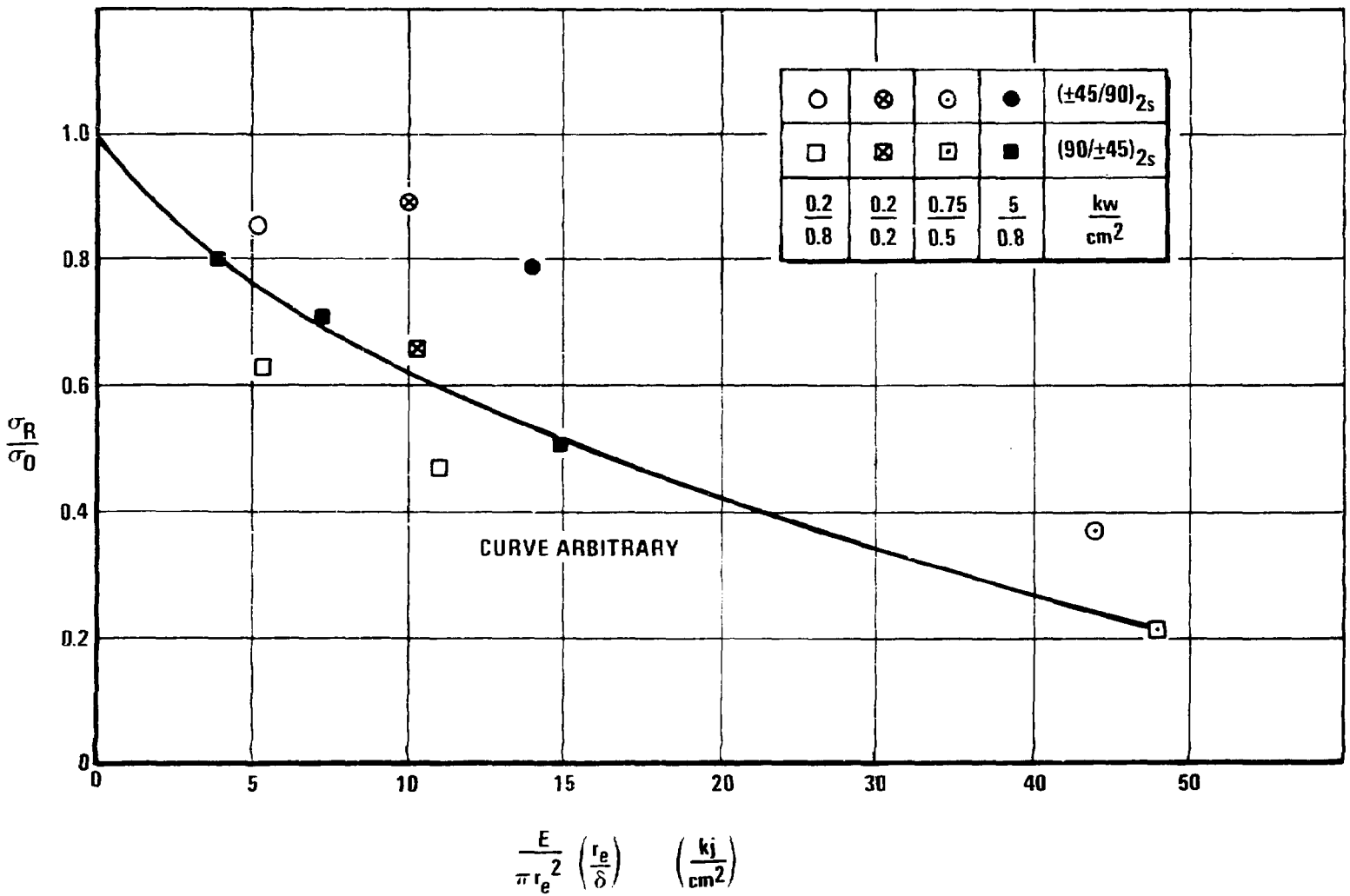

Figure 4-6 Strength Retention for $(90/\pm 45)_c$ vs "Normalized" Energy Density

We note the trend in Figure 4-6 for the $(90/\pm45)_{2S}$ laminates to have greater strength reduction for a given laser exposure than the $(\pm45/90)_{2S}$. This sensitivity to stacking sequence is pronounced over the entire range of exposures considered. The tensile strength for this type of laminate is maximum when about one-third 90's are present (which is the case here). If we consider a low-intensity exposure, for example, where primarily the outer few plies are damaged, we will have a greater change in the effective fraction of 90's present when the 90's are on the outside. In such a case we might expect (as we observe) a greater strength reduction for the $(90/\pm45)_{2S}$. This data thus strongly suggests that attention to stacking sequence (once the lamina percentages have been selected) is important.

4.3.4 Comparative Strength Retentions for $(0/\pm45)_S$ and $(0/\pm45/90)_S$ Laminates

Previous work at General Dynamics (Ref. 1, 2) dealt with laser-damage in a different laminate, $(0/\pm45/90)_S$. It should be of interest to compare those results with the present $(0/\pm45)_S$ laminate data, since both specimen layups contain two plies of 0° fibers.

In Figure 4-7, we repeat the 6-ply strength retention results and indicate the pertinent data from Reference 1. The agreement is quite satisfactory. Note that the old data once again re-enforces our comment about the low intensity "large" beam, i.e., that it is unusually effective at degrading the strength of these coupons. Each of these laminates contains two plies of 0° fibers at the outer surfaces, and we note their strength retentions are quite similar.

4.3.5 Non-Dimensional Parameterization for Laser Damage

It is clear from the preceding figures in this section that the laser-induced strength reduction, follows the trend which one would predict for drilled holes, even when the specimens are not completely penetrated. It thus remains only to choose the parameter which is most useful for modeling and prediction.

It would seem most desirable to describe the results in terms of the incident laser beam characteristics. Then, knowing material parameters such as density and thickness, one might predict the strength retention for a given assumed

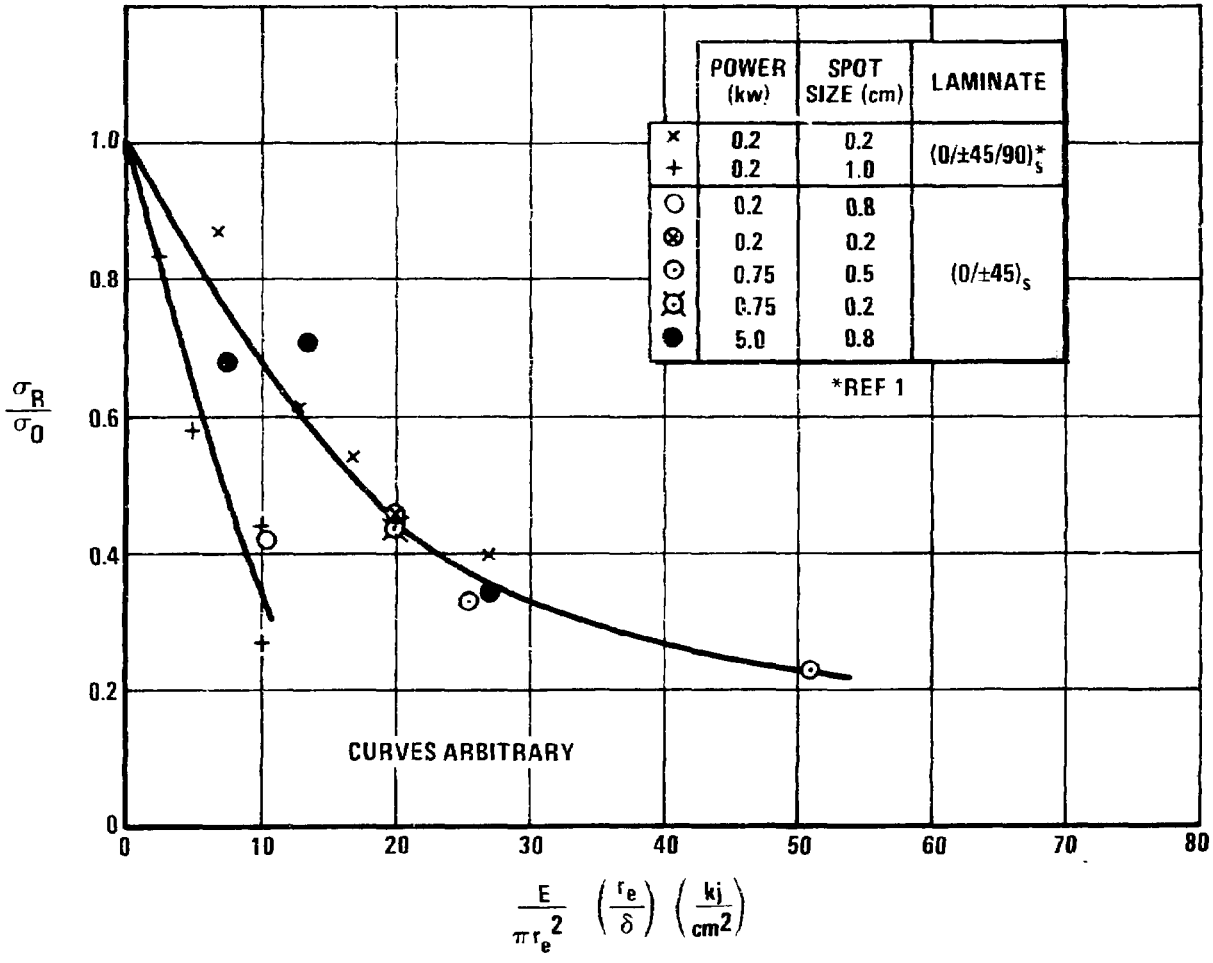

Figure 4-7 Comparison of Strength Retention for $(0/\pm45)_s$ and $(0/\pm45/90)_s$

laser encounter. We suggest then that the basic dependencies required are contained in the parameter $(E/\pi r_e^2)(r_e/\delta)$, for this quantity describes the burn depth (through the energy density factor), the beam size, and adjusts for specimen thickness. With appropriate "constants", this parameter is directly relatable to conventional drilled holes.

To accomplish this link between laser damage and drilled holes, we proceed as follows. In Section 3.5 we noted that a downward extrapolation of the linear part of the $\dot{\mu}(I)$ curve in Figure 3-5 for composites passes near the low intensity points. If we thus assume, to a first approximation, that all our results are dominated by fiber sublimation mass loss, we may proceed as follows. From Eq. 3-23, namely

$$I_S = \frac{1}{\eta} (L_S + \Lambda H) f \dot{\mu}(T), \tag{3-23}$$

and Eq. 3-26,

$$I = P/\pi r^2, \dot{\mu} = \Lambda m/\pi r^2 t_e, \tag{3-26}$$

we may relate incident energy and mass loss. We take $I \approx I_S$, $L_2 = L_S + \Lambda H$, and $r = r_e$ to account for different beam intensity profiles. Then

$$E = Pt_e \approx \frac{1}{\eta} L_2 f \Lambda m,$$

or

$$\frac{\eta E}{f L_2} \approx \Lambda m \tag{4-9}$$

If we assume the mass loss occurs in a cylindrical volume of radius r_e and depth h, then

$$\frac{\eta E}{f L_2} \approx \pi r_e^2 h \rho ,$$

or

$$\frac{\eta E}{\pi r_e^2 \rho L_2 f} \approx h \qquad (4\text{-}10)$$

This equation may be non-dimensionalized by multiplying by $2r_e/w\delta$, where w is the specimen width. This yields the required parameter,

$$\frac{2h}{w}\left(\frac{r_e}{\delta}\right) \approx \left[\left(\frac{2\eta}{\rho f L_2 w}\right)\left(\frac{E}{\pi r_e^2}\right)\right]\left(\frac{r_e}{\delta}\right) , \qquad (4\text{-}11)$$

which represents an effective transverse damage area ratio. In Figures 4-8 and 4-9 we plot σ_R/σ_o for the $(0/\pm45)_c$ and $(90/\pm45)_c$ composites against the parameter on the right side of Eq. 4-11. The solid curves in the figures represent the fracture mechanics-based strength prediction (Eq. 4-1) plotted against the parameter on the left-side of Eq. 4-11. Data is not included for values of the parameter greater than ≈ 0.6, since the prediction is unreliable for large damage-to-width ratios, and the laser-damaged results for that range correspond to data near or at burnthrough.

As noted at the end of Section 3.5, better agreement for the mass ablation correlations would be obtained if the absorptivity η were taken as about 0.75, rather than unity as assumed there. For the data plotted in Figures 4-8 and 4-9, we have taken $\eta = 0.7$, so that the ratio $\eta/f = 1$, where f is the mass fraction of fibers.

The agreement between prediction and results for the $(0/\pm45)_c$ in Figure 4-8 is rather interesting. We note that except for the 200 w/0.8 cm^2 data (open symbols), all results fall essentially on or above the curve. The strength prediction thus apparently gives a lower bound for the strength retention to be expected after a given laser burn in the intermediate to high intensity range. It is not surprising that the open symbol

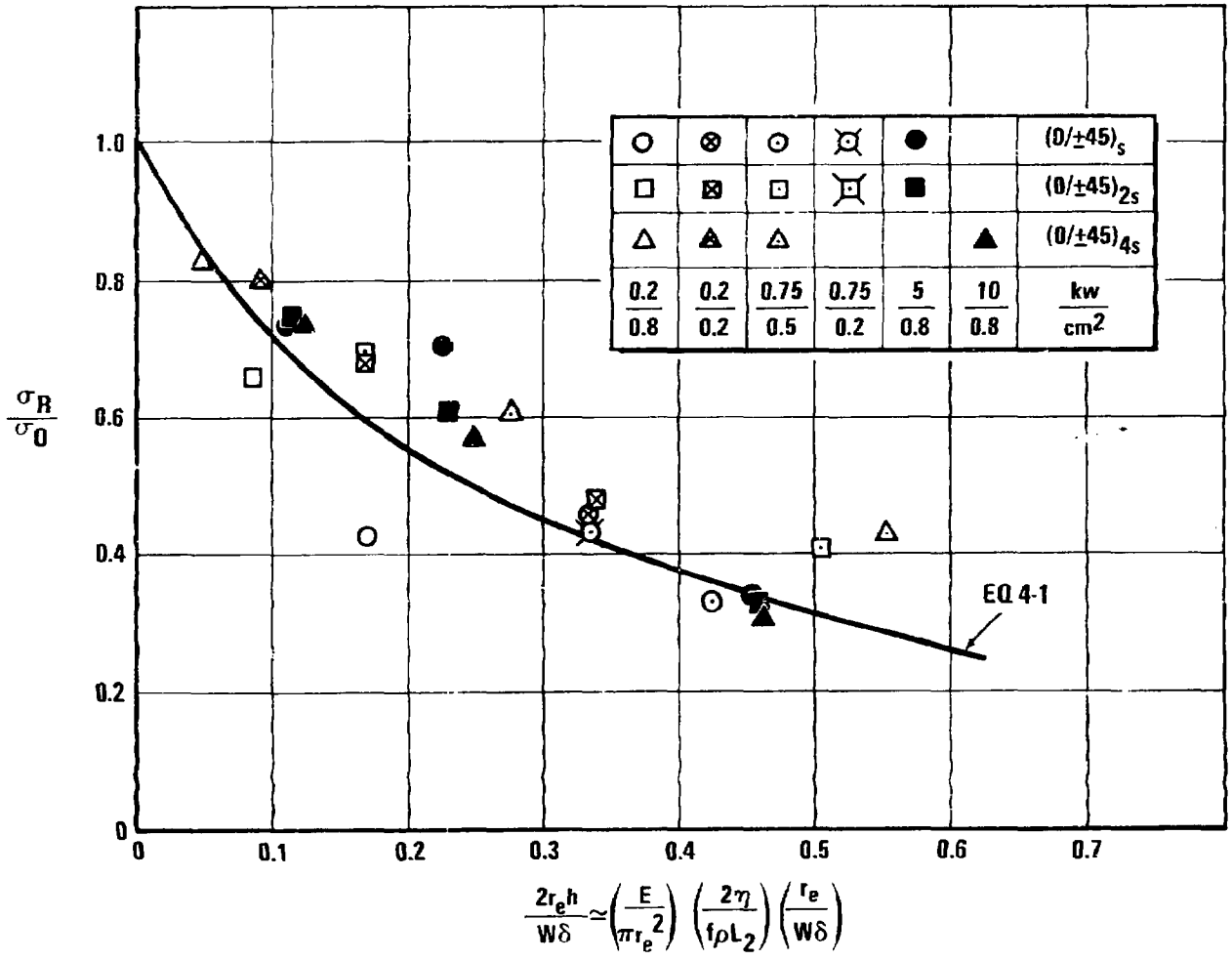

Figure 4-8 Strength Retention for $(0/\pm45)_c$ vs Effective Transverse Burn Area Ratio

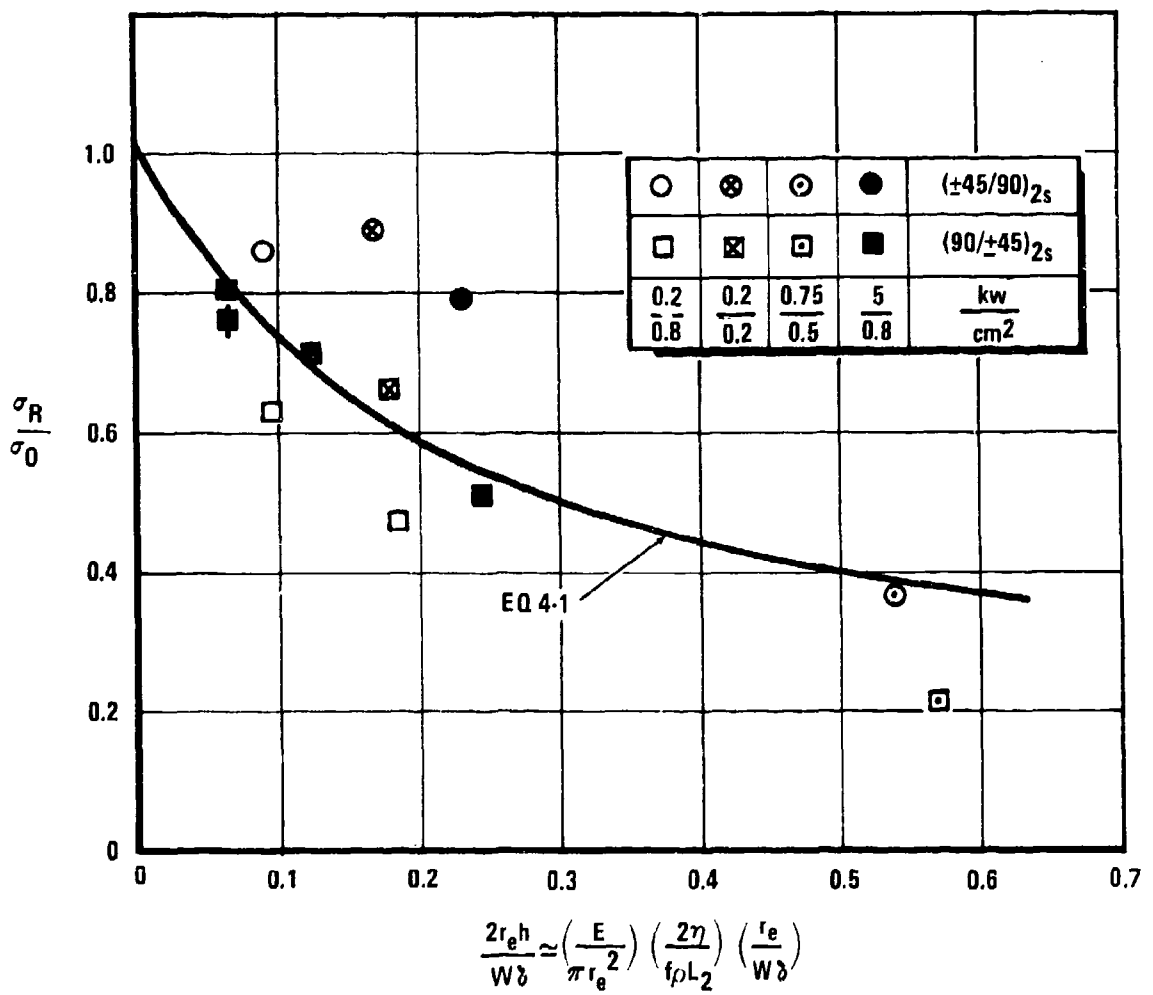

Figure 4-9 Strength Retention for $(90/\pm 45)_c$ vs Effective Transverse Burn Area Ratio

data is distinctly different, for the intensity there is only 250 w/cm^2, well below the expected range of applicability of Eq. 4-11, that is where absorption by graphite sublimation predominates.

Further comment is due regarding the $(0/\pm45)_c$ low intensity results. Two data sets are of particular interest here; 200 w/0.8 cm^2 (250 w/cm^2) and 200 w/0.2 cm^2 (1000 w/cm^2). The latter data is correlated by the parameter of Eq. 4-11, while the former set is not. Recall from Section 3 that in the low intensity range there is no fiber sublimation for exposure times of a few seconds. Since the upper boundary of the low intensity range falls between about 1100 and 1500 w/cm^2, both of these sets of 200 w exposures would formally fall within the low intensity range, though the 1000 w/cm^2 data is near the transition region.

Physically, the specimens damaged with these two intensities differ in the following regard: at 250 w/cm^2 there is no fiber sublimation, but at 1000 w/cm^2 there is actually some fiber removal. It is then reasonable that the 200 watt results with the 0.2 cm^2 spot size (1000 w/cm^2) tend to agree with the higher intensity results, since the model at higher intensity is dominated by fiber sublimation.

The lowest intensity exposures here thus fall experimentally into a separate class where the induced damage is primarily sublimated resin. Results from Ref. 13 cited previously showed that 0° fibers loaded in tension suffer a dramatic reduction in equivalent fiber failure stress if no resin is present to distribute the load. Those data suggest that the local tensile strength of the region of the outer 0° ply from which resin has been removed is about 60 KSI. As such a damaged coupon is loaded in tension, that damaged outer ply is not capable of supporting any load above a very low level. If we view our low intensity $(0/\pm45)_c$ results in this vein, and assume that during testing the tensile load near coupon failure is carried primarily by the undamaged 0° plies, we might expect the strength retention to be proportional to the fraction of undamaged zeroes.

This leads one to expect $\sigma_R/\sigma_o \approx 7/8$, 3/4, and 1/2 for the $(0/\pm45)_{4S}$, $(0/\pm45)_{2S}$, and $(0/\pm45)_S$, since those laminates have, respectively, 8, 4 and 2 plies of 0^o fibers. Note in Figure 4-8 that for the open symbol data those respective strength retentions are approximately 0.83, 0.67, and 0.42, which are not far from the simple predictions above.

Thus, just as the thermal analyses differentiated various thermophysical damage mechanisms in various intensity ranges, we accordingly must note different mechanical failure mechanisms at different intensities. At intermediate and high intensities, the strength retention is predictable by considering fiber sublimation as the dominant mechanism; at low intensity the mere occurrence of resin sublimation from the primary strength determining plies will result in significant strength reduction.

The results for the matrix-dominated $(90/\pm45)_S$ are shown in Figure 4-9 with the strength prediction of Eq. 4-1 for those laminates. Less data were obtained for these laminates and the scatter is evident. The prediction does follow the trend of the results. The feature to note there again is the sensitivity of the strength retention to the stacking sequence. For equivalent exposures, the $(90/\pm45)_{2S}$ have lower strength retention than the $(\pm45/90)_{2S}$.

4.4 AIRFLOW EFFECTS

For the experimental conditions used in this program, there is little effect of airflow conditions on strength retention in the composite specimens. One such airflow comparison for aluminum presents a different picture. Table 4-5 summarizes the major variations in airflow conditions used in this program.

Table 4-5 Effect of Airflow on Strength Retention

Specimen	Energy Density (kj/cm^2)	Airflow (M)	σ_R/σ_o
$(0/\pm45)_{4S}$	10.2	0.3	0.57
$(0/\pm45)_{4S}$	10.2	0.9	0.54
$(0/\pm45)_{4S}$	9.6	0.1	0.61
$(90/\pm45)_{2S}$	1.28	0.3	0.80
$(90/\pm45)_{2S}$	1.28	None	0.76
Aluminum	2.55	0.3	0.51

For these high intensities, radiative emission is negligible compared to sublimation absorption in the composites, and forced convection cooling effects are expected to be smaller than the radiative emission term. We thus would expect little, if any, airflow effect. Note that for the $(0/\pm45)_{4S}$, as the airflow increases, σ_R/σ_o decreases slightly; but for the $(90/\pm45)_{2S}$, the reverse is indicated. Neither of these variations in strength retention is significant however, since the range of variation in residual strengths for "identical-damage" specimens is typically $\pm5\%$.

Since the heat of sublimation for aluminum is considerably less than that of graphite, we might expect a measurable change in damage under different airflow conditions. The aluminum comparison in Table 4-5 indicates this change. A significant improvement in strength retention (and much smaller mass loss) is noted at high airflow conditions for the aluminum specimens.

Airflow effects were also considered by Kibler in Reference 14, where graphite-epoxy skin $(0/\pm45)_S$/honeycomb sandwich compression beams were irradiated under conditions similar to those in the present program. One additional feature was included in that work, however: large beam ($\approx 10 cm^2$) irradiations. The results there indicated that, for beam spot sizes of the order of 0.9 cm^2, increased airflow tends to slightly increase residual compression strength. For the 10 cm^2 beam however, the strength retention was decreased slightly with higher airflow. The inference drawn was that given an incident beam condition which destroys significant areas of the epoxy matrix and removes fiber support, the damage may be amplified at high Mach numbers (0.9M) where surface fibers may be blown off. Such an effect might be relatively unimportant with small spot sizes due to the limited damage area.

4.5 COMPARISON OF STRENGTH RETENTION FOR GRAPHITE-EPOXY COMPOSITES AND ALUMINUM

In this subsection, we will compare two aspects of laser damage in composites with that in aluminum: penetration times and residual tensile strength. The 2024(T81) aluminum coupon thickness, 0.090 inch (0.229 cm) was selected to give an unnotched load capability approximately the same as the $(0/\pm45)_{2S}$ graphite-epoxy laminates (δ = 0.185 cm). The average failure loads were not as close as expected, however, being about 6600 lb and 5500 lb for the aluminum and composite respectively. The ultimate tensile strengths were similar: 73.2 ksi for the aluminum and 76.9 ksi for this particular laminate.

Figure 4-10 summarizes the high intensity burnthrough measurements on aluminum and two thicknesses of graphite-epoxy composite. These data were previously used in Section 3 for the thermal characterization, but are presented here for ease of comparison. The thicknesses for these burnthrough specimens are slightly different from those of the tensile coupons, but the results are clear. At 5 kw, the penetration time for the aluminum is about 40% of that for the composite, even though the aluminum in this case is about 40% thicker. In this intensity range, the thermal analyses indicate a small contribution to the composite response by radiative emission. At 10 kw, both

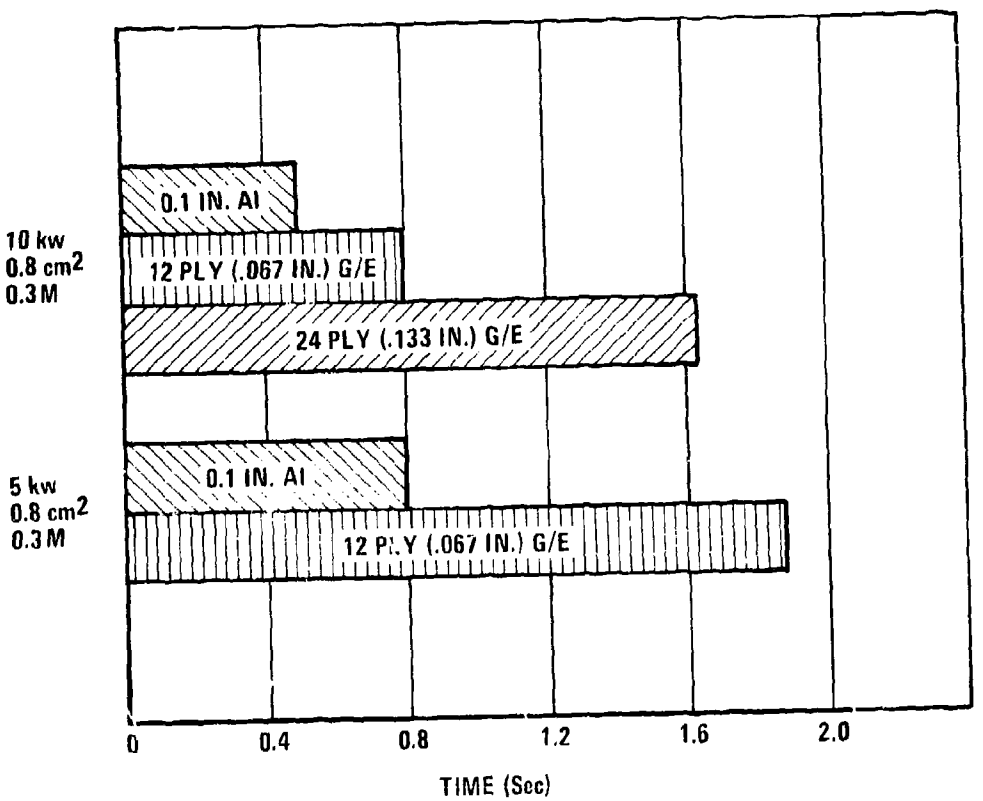

Figure 4-10 Burnthrough Times

the composite and aluminum responses are completely controlled by heats of sublimation, so the times are more nearly the same. One can also note in this figure the exposure-time dependence for burnthrough of different thicknesses of composite. At 10 kw, the burnthrough time is twice as long for the 24 ply as for the 12 ply laminate.

In Figure 4-11 we compare the tensile strength retention σ_R/σ_o, for the laser damaged aluminum and composite coupons. The data are there plotted against the parameter $(E/\pi r_e^2)(r_e/\delta)$ which has units of energy density and includes the specimen thickness. It is not particularly useful in such a comparison of dissimilar materials to include factors such as material density and absorptivity. The curves drawn are arbitrary. In the case of the composite data, e.g., the curve roughly indicates the lower boundary of strength retention.

With the 200 watt beam exposures we see the effects of the comparatively high thermal conductivity of the aluminum. For these intensities, it is not possible to degrade the aluminum. Indeed the specimens show only slight discoloration of the paint.

With the 750 watt beam, we note that the strength retention is roughly equivalent for the composite and aluminum. The solid data points (5 kw beam) present a different picture. For a given exposure, the aluminum strength retention is typically 60% of that for the composite for the range of exposures compared. This result is quite reasonable in terms of our thermal analyses, for at these high intensities we expect "sublimation cooling" to be important for the composite, so that it takes disproportionately greater energy absorption to inflict greater damage. This effect is not as important at 750 watts, e.g., and the induced damage is similar for the aluminum and composite.

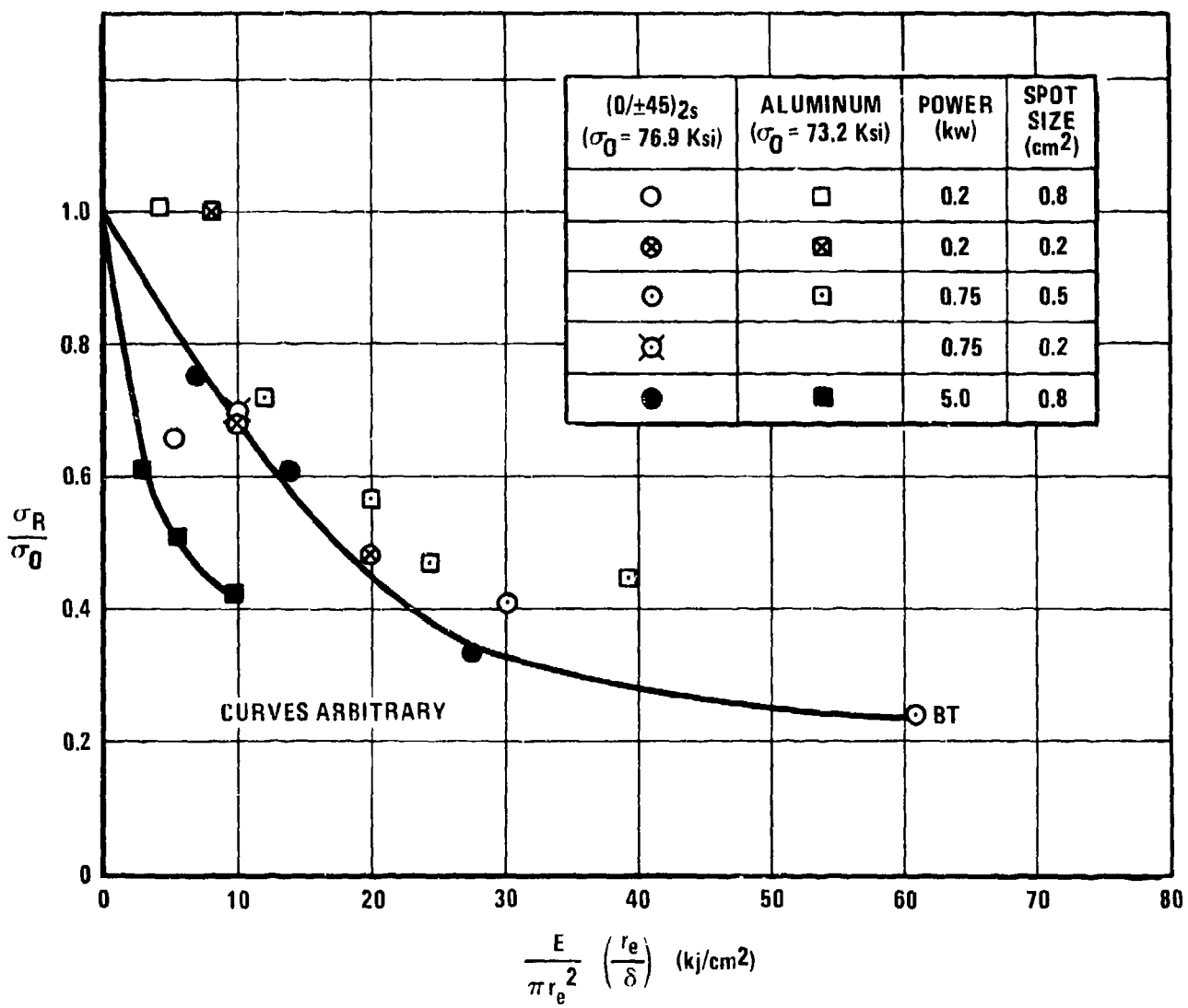

Figure 4-11 Comparison of Strength Retention for Laser-Damaged 2024(T81) Aluminum and 5208/T300 $(0/\pm45)_{2s}$ Composite

4.6 IRRADIATION OF PRELOADED SPECIMENS

In Figure 4-12 we have plotted all data for composite and aluminum specimens irradiated under tensile loading. The solid points are plotted at coordinates representing the preload σ_F/σ_o (fraction of ultimate) and the energy density at fracture. The open points represent the residual strengths σ_R/σ_o of the specimens which did not fail when loaded at the indicated σ_F/σ_o and irradiated with the indicated energy density (dotted lines). For both the aluminum and composite specimens, the solid curves are taken from Figure 4-11. The dotted curve defines the approximate preload/laser exposure conditions required for catastrophic failure of the composites.

We note that for a given incident energy density, a specimen under load will fracture at 75-95% of the value of residual strength it would have had it not been loaded. For the composites, it appears that if the specimen does not fracture under irradiation while loaded, its residual strength will be similar to that for an unloaded specimen which experienced the same irradiation.

An interesting feature of the composite specimens which fractured at a preload of 0.5 is that the two dry ones fractured at noticeably lower energy levels than the one which contained about 0.7% moisture. Although it is unwise to draw much from such few data, it is tempting to suggest that the somewhat plasticized resin in the wet specimen is more forgiving of damage than the more brittle dry resin.

For comparison purposes we have plotted, in Figure 4-13, data from Reference 2. A quasi-isotropic laminate was used there with laser exposures similar to the present program. We note that the 200 w/0.2 cm^2 data cluster well around the curves (repeated from Figure 4-12), but the 200 w/1cm^2 results show a trend to fracture at somewhat lower incident energy density for a given preload. This brief comparison does serve to re-emphasize a point made earlier. Low intensity exposures in a relatively large spot are disproportionately effective for inducing damage in graphite epoxy composites.

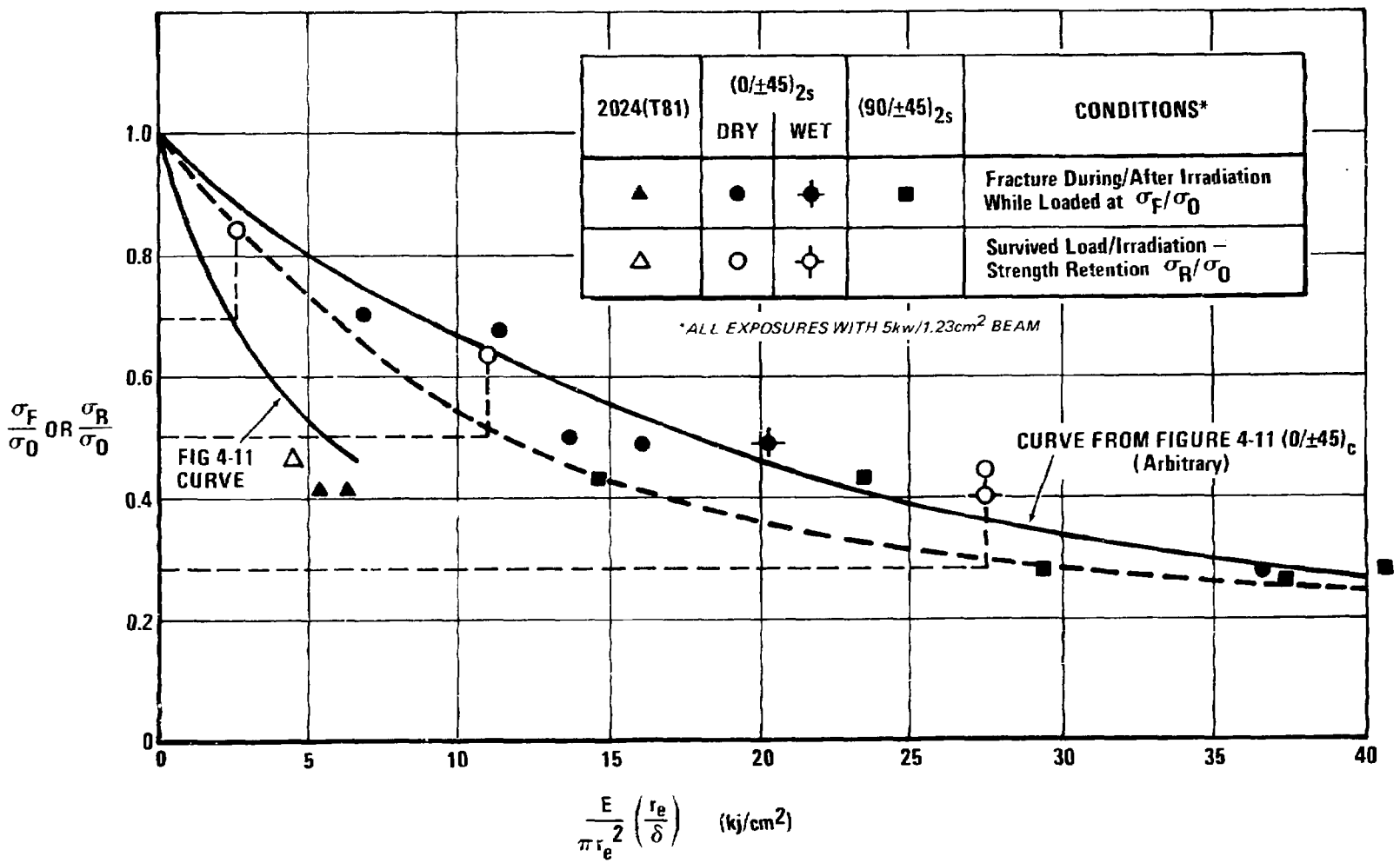

Figure 4-12 Irradiation of Preloaded Specimens

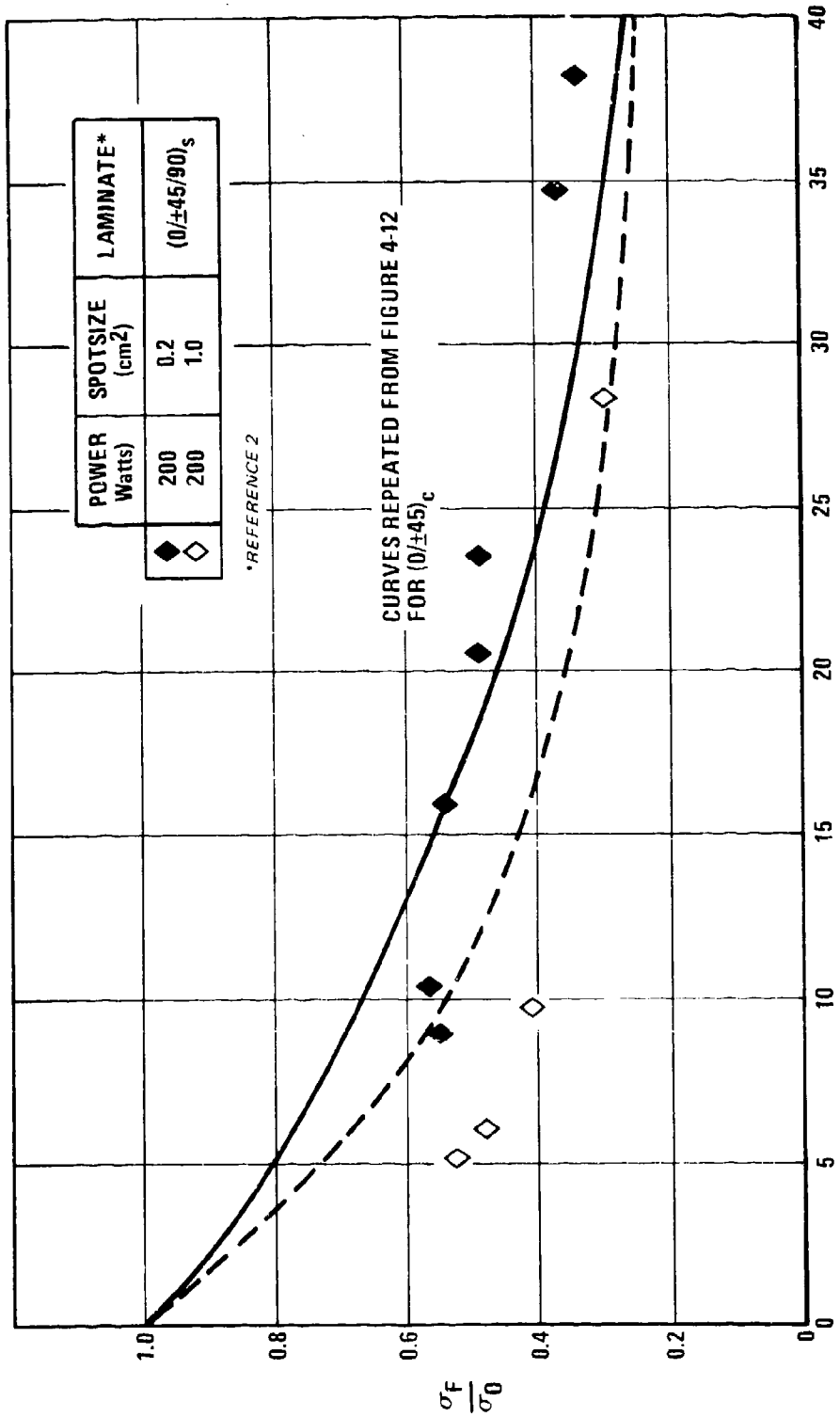

Figure 4-13 Comparison of Preloaded $(0/\pm45)_c$ and $(0/\pm45/90)_s$

4.7 NOTE ON TENSION VS. COMPRESSION STRENGTH RETENTION

Kibler (Ref. 14) investigated the laser-induced reduction in residual compressive strength in honeycomb sandwich beams with $(0/\pm45)_S$ skins so it is interesting to compare those results with our $(0/\pm45)_S$ tension results.

At first thought, one might expect the following behavior for a damaged beam tested in compression. No matter how little energy is incident on the skin, as long as the epoxy matrix is damaged at the outer ply, the 0^o fibers will not support compressive load. The damaged outer ply will thus fail first, and the residual compressive strength might be expected to be directly proportional to the size of the surface damaged area. This description is not far from the actual situation. Those results suggest that laser damage to the outer ply causes an immediate reduction in residual strength by about 50%. As the exposure time, or equivalently, absorbed energy increases, strength reduction proceeds more slowly.

The interesting feature of the compression data is that, if plotted against our energy density parameter, $\frac{E}{\pi r_e^2}\left(\frac{r_e}{\delta}\right)$, the compressive strength retention does generally follow the tensile results for the same laminate for the exposure conditions considered.

Both sets of data (and the $(90/\pm45)_c$ results from Section 4.3.3) would suggest that altering the stacking sequence (while retaining the required percentages of each orientation) of a laminate might be effective in improving its strength retention after laser exposure.

4.8 SUMMARY OF MECHANICAL CHARACTERIZATION

We have shown in the preceding paragraphs that the strength retention of laser-damaged composites is conveniently described by a parameter which depends on incident energy density, incident beam radius, and specimen thickness. The results may be expressed in dimensionless form by writing the parameter as

$$\left[\left(\frac{E}{\pi r_e^2}\right)\left(\frac{\eta}{f \rho L_2}\right)\right]\left(\frac{2r_e}{w\delta}\right) \approx h \frac{2r_e}{w\delta} \qquad (4\text{-}11)$$

where the term in brackets on the left side of Eq. 4-11 describes an effective penetration depth. In this form, the parameter characterizes an effective transverse damage cross section, and thus may be related to drilled holes as indicated by the right side of Eq. 4-11.

A fracture-mechanics-based strength prediction based on our notched control data adequately describes the laser-damaged strength retention of $(0/\pm45)_c$ laminates at all except the lowest beam intensity investigated. At low intensity, the damage is due to resin sublimation with no fiber removal, and thus represents a separate response, both from a thermal and mechanical standpoint. Sublimation of the resin from the outer 0^o ply does however effectively limit the load capability of that ply, resulting in significant strength reduction without fiber ablation.

The $(90/\pm45)_c$ matrix-dominated laminate results are generally predictable using the same parameterization as above, although the experimental data scatter is large. Different strength retentions were noted for the two different stacking sequences of this laminate class, which emphasizes the relative sensitivity of laser-damaged residual strength to near-surface ply orientation.

Airflow variation in the ranges considered (0.1M - 0.9M) has little effect on subsequent strength retention of laser damaged composites. We suggest however that airflow may be important at significantly large beam spot sizes.

With regard to burnthrough times for high intensity beams, 2024(T81) aluminum is more easily penetrated than graphite-epoxy coupons of approximately equivalent undamaged strength. With respect to laser-damaged strength retention, the aluminum/composite comparison must be discussed in the three intensity ranges used in Section 3. At low intensity, the aluminum is not damaged and no strength reduction occurs. In the intermediate intensity range, the strength retentions are similar for both composites and aluminum coupons. At high intensity, the aluminum retention is typically 60-70% of that for the composite similarly exposed.

Preloaded composites and aluminum tend to fracture under laser exposure at loads equivalent to approximately 75%-95% of the strength retention they would have if similarly exposed without load. If the preloaded/irradiated specimens are not exposed until time of fracture, their residual strengths are similar to those for unloaded specimens equivalently irradiated.

5. CONCLUSIONS AND RECOMMENDATIONS

The overall goal of this program was to develop a basic understanding of the response of graphite-epoxy materials to laser radiation. In this section we discuss (1) fulfillment of this goal in terms of general conclusions reached, and (2) recommendations for future work based on the present program results.

5.1 CONCLUSIONS

Although a graphite-epoxy material system is unquestionably complex, the thermophysical mechanisms of laser-induced damage are understandable and predictable. By considering the material response in various incident intensity ranges, we have delineated the interactions which occur and formulated models which predict the thermal response, mass ablation, and penetration in those ranges. The understanding of material thermal response has allowed us to correlate the strength retention after various laser exposures with incident beam characteristics, and has provided a basis for differentiating the mechanical degradation induced by different beam intensities.

We have determined that, while no damage occurs in aluminum at low intensity, the aluminum is more susceptible than composites to damage at high intensity. Both penetration time and strength retention are less for aluminum than composites at high intensity. At intermediate intensities, the strength retentions are similar for these two materials.

The strength retention for partially-penetrated, laser-damaged composites is describable in terms of fracture-mechanics-based predictions at all but the lowest intensity considered. The criterion for this predictability relates to whether only resin, or resin plus fiber, sublimation occurs. If the latter is true, all fiber-dominated strengths are correlated by a dimensionless parameter which involves beam intensity, beam spot size, specimen thickness, and an

effective heat of ablation. If only resin sublimation occurs, the prediction over-estimates the strength retention. By considering different stacking sequences of the same class of laminates, we have shown that the strength retention is sensitive to stacking for partial-penetration damage.

If specimens are loaded in tension and irradiated to failure, they will fracture at a preload fraction which is not drastically less than the strength retention of similarly-exposed, but unloaded specimens. If the irradiation of pre-loaded specimens is terminated before fracture, their residual strengths will be similar to equivalently-exposed unloaded specimens.

Variations in airflow do not seem significant for the experimental conditions used, inasmuch as the successful thermal analyses were conducted without consideration of convective cooling. We suggest however that airflow variation, particularly toward higher Mach numbers, may influence the damage with larger beam spot sizes.

5.2 RECOMMENDATIONS

The present work has considered basically one material system (5208/T300) in a variety of thicknesses and stacking sequences over a wide range of incident laser beam intensities. As a comparison, the work of Ender, et al (Ref. 3) considered several material systems, with essentially one thickness per material, over the intermediate to high intensity range, as here defined. These two investigations yield consistent results when compared under similar experimental conditions. It is apparent now that the response of certain materials to laser radiation is reasonably well understood at intermediate to high intensities.

From our work on this program, it is evident that further attention is needed to the mechanical response of composites to low intensity laser radiation. The thermal response there is characterized primarily by resin sublimation, with little apparent fiber damage for exposure times on the order of

seconds. The strength reduction however, can be considerable. The role of the resin in a laminate is reasonably well understood in general terms, but further experimental and analytical detail is required to predict the strength retentions of resin-damaged laminates.

Early work at low intensity (Ref. 1) indicates that the strength retention there is relatable to fracture-mechanics-based predictions as we have here employed; time did not permit exploration of the link between low-and high-intensity mechanical results here however.

We would therefore strongly recommend further investigations of laser-induced strength reduction in graphite-epoxy materials under large beam, low intensity exposures, including examination of the stacking sequence sensitivities.

As part of these investigations, two further areas appear fruitful for consideration. Since our low-intensity thermal analyses successfully predicted back surface temperatures during exposures, one could use through-the-thickness thermal gradient calculations to predict thermally-induced interlaminar normal stresses. The role of these stresses in subsequent strength reduction could then be both analytically and experimentally considered. The other area of investigation would examine the fatigue behavior of low-intensity-damaged composites. Notched composites generally show little sensitivity to tension fatigue when loaded in the fiber direction; in compression-dominated fatigue, however, severe degradation may occur. The effects of both types of fatigue loading on laser-damaged composites bear thoughtful examination.

6. REFERENCES

1. K. G. Kibler, H. G. Carter, and J. R. Eisenmann, "Residual Strength of Laser-Damaged Composites," Journal of Composite Materials 9, 28 (1975)

2. K. G. Kibler and H. G. Carter, "Laser Damage in Graphite-Epoxy Composites," General Dynamics Research Report ERR-FW-1564 (15 October 1974)

3. T. Ender, H. T. Clark, and T. C. Grimm, "Response of Advanced Fiber Composite Materials to Laser Heating (U)," McDonnell Douglas Corporation Report MDCA 3540 (1975) (Confidential)

4. M. E. Waddoups, J. R. Eisenmann, and B. E. Kaminski, "Macroscopic Fracture Mechanics of Advanced Composite Materials," Journal of Composite Materials 5, 446 (1971)

5. L. Pauling, The Nature of the Chemical Bond Cornell University Press, (1960) p85

6. R. E. Honig, "Mass Spectrometric Study of the Molecular Sublimation of Graphite", J. Chem Phys 22 126 (1954)

7. R. J. Thorn and G. H. Winslow, "Vaporization Coefficient of Graphite and Composition of the Equilibrium Vapor" J. Chem Phys 26 186 (1957)

8. E. W. Washburn, International Critical Tables Vol 5, McGraw-Hill (1929) p53

9. J. R. Eisenmann, "Bolted Joint Static Strength Model for Composite Materials," NASA TM X-3377, Third Conference on Fibrous Composites in Flight Vehicle Design, April, 1976

10. J. P. Waszczak, "A Synthesis Procedure for Mechanically Fastened Joints in Advanced Composite Materials," AFML-TR-73-145, Volume II, September, 1973

11. R. J. Nuismer and J. M. Whitney, "Uniaxial Failure of Composite Laminates Containing Stress Concentrations," presented at ASTM Conference on Fracture Mechanics in Composites, Gaithersburg, MD, 25 September 1974

12. J. M. Whitney and R. Y. Kim, "High Temperature Tensile Strength of Graphite/Epoxy Laminates Containing Circular Holes," Journal of Composite Materials 10, 319 (1976)

13. E. L. McKague, Jr., "Development of a Graphite Fiber Tow Test Method," General Dynamics Research Report ERR-FW-1588 (December 1974)

14. K. G. Kibler, "Laser-Induced Strength Reduction in Graphite-Epoxy Compression Sandwich Beams," General Dynamics Research Report ERR-FW-1795 (1976)